environmental microbiology

Environmental Microbiology (2017) **19**(10), 3863–3878 doi:10.1111/1462-2920.13743

Taxonomic variability and functional stability in microbial communities infected by phages

Stilianos Louca[1,2]* and Michael Doebeli[1,2,3]

[1]*Biodiversity Research Centre, University of British Columbia, Canada.*

[2]*Department of Zoology, University of British Columbia, Canada.*

[3]*Department of Mathematics, University of British Columbia, Canada.*

Summary

Microbial communities can display large variation in taxonomic composition, yet this variation can coincide with stable metabolic functional structure and performance. The mechanisms driving the taxonomic variation within functional groups remain largely unknown. Biotic interactions, such as predation by phages, have been suggested as potential cause of taxonomic turnover, but the conditions for this scenario have not been rigorously examined. Further, it is unknown how predation by phages affects community function, and how these effects are modulated by functional redundancy in the communities. Here, we address these questions using a model for a methanogenic microbial community that includes several interacting metabolic functional groups. Each functional group comprises multiple competing clades, and each clade is attacked by a specialist lytic phage. Our model predicts that phages induce intense taxonomic turnover, resembling the variability observed in previous experiments. The functional structure and performance of the community are also disturbed by phage predation, but they become more stable as the functional redundancy in the community increases. The extent of this stabilization depends on the particular functions considered. Our model suggests mechanisms by which functional redundancy stabilizes community function and supports the interpretation that biotic interactions promote taxonomic turnover within microbial functional groups.

Received 30 September, 2016; revised 16 March, 2017; accepted 24 March, 2017. *For correspondence. E-mail louca@zoology.ubc.ca; Tel. +1 604 512 9794.

Introduction

Microbial communities can exhibit strong variation in taxonomic composition, both across time and space. However, this taxonomic variation may often coincide with remarkably stable functional community structure (Dumont *et al.*, 2009; Ofiţeru *et al.*, 2010; Rodriguez-Brito *et al.*, 2010; Louca *et al.*, 2016a). For example, the proportions of several metabolic functional groups, such as nitrifiers, phototrophs and sulfate reducers, were found to be similar across replicate natural aquatic ecosystems despite strong taxonomic turnover within individual functional groups (Louca *et al.*, 2016a). Similarly, methanogenic, methanotrophic and nitrifying bioreactors operated under constant conditions were found to exhibit intense turnover of bacterial operational taxonomic units (OTUs) despite constant overall biochemical performance (Fernández *et al.*, 1999; Fernandez *et al.*, 2000; Wittebolle *et al.*, 2008; Wang *et al.*, 2011; Fernandez-Gonzalez *et al.*, 2016). These observations point towards an elegant paradigm in microbial ecology, in which energetic and stoichiometric constraints determine functional community structure and performance, but a high degree of functional redundancy in the regional OTU pool enables taxonomic variability within individual functional groups. The mechanisms driving this taxonomic variability remain poorly understood. Neutral population drift between equivalent competitors is sometimes suggested as a possible cause (Ofiţeru *et al.*, 2010), however non-random phylogenetic structure and co-occurrence patterns within functional groups point towards deterministic mechanisms, notably biotic interactions (Louca *et al.*, 2016a). In some cases, complex community trajectories have been reproduced across replicate isolated systems under constant conditions (Vanwonterghem *et al.*, 2014), further suggesting that the taxonomic turnover within functional groups need not be stochastic.

Host-specific predation by lytic phages has been suggested as a potential mechanism promoting host succession through 'killing the winner' (KTW) dynamics, in which abundant host populations eventually collapse due to increased predation, giving way to opportunistic competitors (Middelboe *et al.*, 2001; Rodriguez-Valera *et al.*, 2009; Vos *et al.*, 2009; Rodriguez-Brito *et al.*, 2010; Shapiro and Kushmaro, 2011). Previous experiments

revealed strong OTU turnover in a bioreactor, in which the temporary emergence of specific OTUs was followed by the temporary increase in their specific phages, consistent with KTW dynamics (Shapiro *et al*., 2010). Predation by lytic phages is increasingly recognized as an important contributor to microbial mortality in natural and engineered ecosystems (Middelboe *et al*., 2001; Thomas *et al*., 2011). Cell lysis has been shown to reduce the flux of assimilated organic carbon to higher trophic levels such as protist grazers (Fuhrman, 1999; Weitz *et al*., 2015) and is believed to enhance nutrient recycling and storage in the ocean surface (Jover *et al*., 2014; Weitz *et al*., 2015), although aggregate formation by viral lysis may increase carbon sinking in the water column (Guidi *et al*., 2016). The effects of phages on non-assimilatory carbon fluxes (e.g. fluxes for energy gain) are much less understood (Shapiro and Kushmaro, 2011), despite the fact that in many (e.g. methanogenic) environments most organic carbon is metabolized to byproducts for energy gain rather than assimilated into cell mass (McDuffie, 1991). Further, it is unclear whether – and under what conditions – phage-driven KTW dynamics can fully explain the discrepancy between taxonomic variability and functional stability observed in microbial communities (Dumont *et al*., 2009; Ofiţeru *et al*., 2010; Rodriguez-Brito *et al*., 2010; Louca *et al*., 2016a). While this role of KTW dynamics is often hypothesized, in practice time lags involved in the recovery or replacement of collapsed populations, as well as potentially destabilizing interdependencies between pathways in complex metabolic networks, could prevent the functional stability of communities.

To elucidate the effects of phage predation and microbial functional redundancy on community structure and metabolic functioning, we constructed a mechanistic model for a methanogenic microbial community subject to predation by lytic phages, hosted within a flow-through bioreactor. Bioreactors constitute powerful model ecosystems for microbial ecology, because physicochemical conditions can be closely monitored and controlled, enabling replicate time series experiments. It is thus not surprising that bioreactor experiments have greatly contributed to our mechanistic understanding of microbial communities and of phage-host dynamics in particular (McDuffie, 1991; Fernández *et al*., 1999; Ofiţeru *et al*., 2010; Shapiro and Kushmaro, 2011). We chose methanogenic systems as an example because these are relatively well understood and of great environmental as well as industrial relevance (Conrad, 1999; Hashsham *et al*., 2000), and because this allows for comparisons with previous experiments (Fernández *et al*., 1999; Fernandez *et al*., 2000; Vanwonterghem *et al*., 2014; 2016).

Our model considers the dynamics of multiple microbial populations driving the anaerobic catabolism of glucose (the input substrate) to methane (CH_4). Following Conrad (1999), this catabolic process can be roughly separated into three stages: In the first stage glucose is fermented to short-chain fatty acids, lactate and alcohols. In the second stage, these fermentation products are further catabolized to hydrogen (H_2) and acetate by syntrophs, i.e. bacteria that rely on a rapid consumption of H_2 and acetate in a third stage, which in turn is performed by hydrogenotrophic (H_2/CO_2) and acetoclastic methanogenic archaea. In our model, each of these three stages (fermentation, syntrophy, methanogenesis) comprises multiple alternative metabolic reactions (12 reactions in total, overview in Fig. 1 and Supporting Information Table S1). We identify each of these reactions as a distinct function, and each function is performed by a distinct microbial 'functional group' that may comprise one or more distinct cell lineages – henceforth referred to as operational taxonomic units (OTU). OTUs within the same functional group catalyze the same reaction but differ randomly in several of their physiological parameters, such as their substrate half-saturation constants or maximum growth rates (overview in Supporting Information Table S2). We use 'OTU' as an abstract taxonomic group (such as a strain or species) that is sufficiently narrow so that reaction kinetics are similar across members, and sufficiently broad so that different OTUs are infected by different specialist phages (Paez-Espino *et al*., 2016). The number of OTUs initially present in each functional group (termed 'functional redundancy') is a key parameter in our analysis and accounts for the presence of multiple functionally similar clades in many ecosystems (Wohl *et al*., 2004; Ofiţeru *et al*., 2010; Louca *et al*., 2016a,b). Note that here functional redundancy refers to the number of OTUs at the beginning of our simulations (i.e. in the inoculum, the available 'seed bank'),

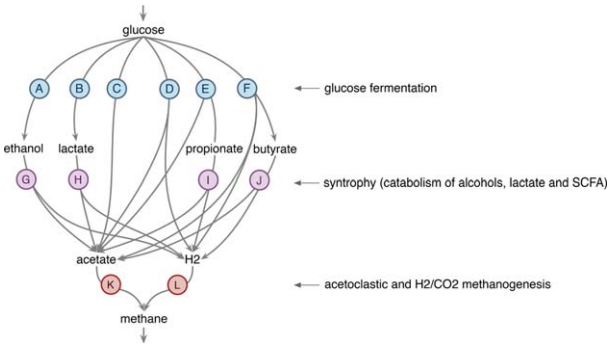

Fig. 1. Modelling methanogenic communities.
Simplified metabolic network of anaerobic methanogenic communities (Conrad, 1999), as modelled in this study. Each circle represents a functional group that is specialized on a particular metabolic reaction, and each functional group can comprise multiple competing OTUs ('functional redundancy'). The network is structured into three sequential catabolic stages based on the type of substrate used (fermentation, syntrophy and methanogenesis). Detailed reaction stoichiometry in reference to the inscribed letters is provided in Supporting Information Table S1. [Colour figure can be viewed at wileyonlinelibrary.com]

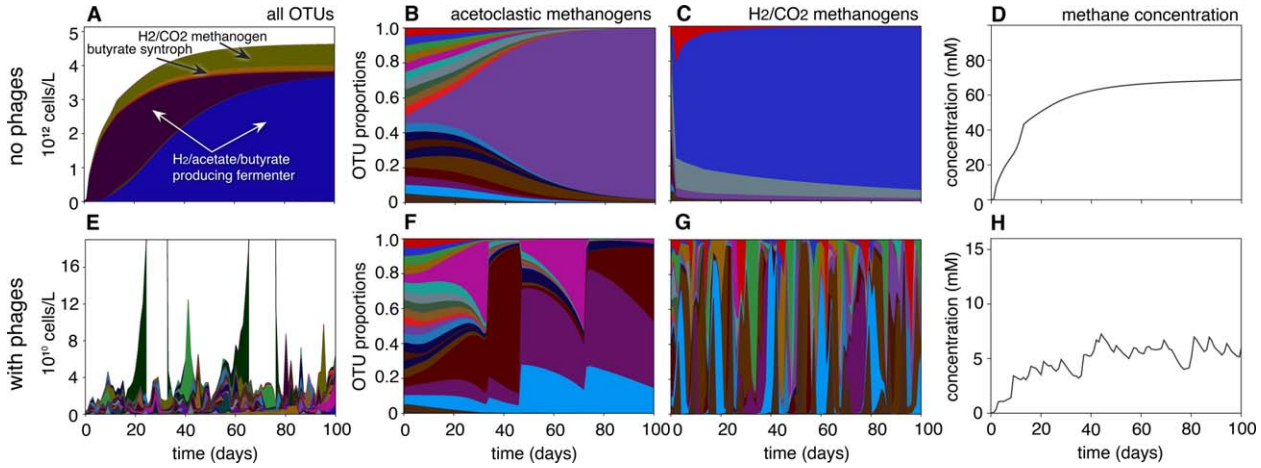

Fig. 2. Phage predation drives OTU turnover.
(A) OTU abundances (one colour per OTU) during a single simulation without phage predation, at 20-fold functional redundancy in the inoculum. Competitive exclusion eventually leads to the extinction of almost all OTUs, with the exception of a single fermenter and two methanogens. (B, C) Proportions of (B) acetoclastic methanogens and (C) of H_2/CO_2 methanogens (one color per OTU). (D) Methane concentration in the effluent. All plots A–D were generated by the same simulation. (E–H): Analogous to (A–D), but for a simulation including phage predation. Phage-host interactions drive variation in overall cell abundances (E) as well as in the OTU composition within functional groups (F,G). [Colour figure can be viewed at wileyonlinelibrary.com]

while we make no assumptions regarding the long-term persistence of any OTU. Each OTU is associated with a distinct phage population that infects cells and causes increased mortality through cell lysis. Cell infection rates are proportional to phage concentrations and phage population growth is, in turn, driven by the release of phage particles during cell lysis. Cell lysis also leads to the release of organic carbon (glucose) and nitrogen (ammonium, an additional resource in our model), which become again available for catabolism and assimilation (Azam, 1998). Physiological parameters were chosen randomly for each OTU and each phage within realistic ranges (Supporting Information Table S2), to account for the variation typically seen between strains or species (Ohtsubo *et al.*, 1992; Mladenovska and Ahring, 2000). As we describe below, our model successfully reproduces previous experimental observations and yields novel insight into the effects of phage predation and functional redundancy on microbial community composition and function.

Results and discussion

Bioreactor dynamics in the absence of phages

Following 'startup' of the bioreactor, and in the absence of phages, the successive growth of fermenters, syntrophs and methanogens quickly leads to the stabilization of metabolic activity within a few weeks (Fig. 2A). At this stage, microbial metabolism balances glucose supply and residual substrate loss from the bioreactor, although the exact steady state metabolite concentrations and community composition depend on the random parameters chosen. In most simulations glucose consumption was nearly complete, and overall community function (in terms of methane production) was constrained by glucose supply ('bottom-up' control). Competitive exclusion between reactions that are limited by the same substrates eventually leads to the persistence of only a subset of possible pathways driving glucose catabolism to CH_4 and CO_2. Each reaction is eventually performed by at most one remaining OTU in the corresponding functional group (Figs 2B and C), and this OTU is characterized by its ability to persist at the lowest substrate concentration (Tilman, 1982). Some functional groups may go completely extinct. The bulk of biomass is attributable to fermenters and, to a lesser extent, syntrophs. Methanogens only account for a small fraction ($\sim$1−10 %) of the community, consistent with experimental observations (Vanwonterghem *et al.*, 2016), because most of the energy available from glucose catabolism is harvested in the preceding steps (Conrad, 1999).

Effects of phages on community dynamics

When phages are included in the model, communities exhibit intense succession of distinct host populations that bloom temporarily and eventually collapse due to increased predation by phages (Fig. 2E). The duration of each infection period (i.e. from the initial detection to the eventual collapse of a phage population) varies greatly between phage-host pairs and between simulations, but is typically on the order of a few days, consistent with time scales of phage population dynamics observed in bioreactors (Weinbauer, 2004; Barr *et al.*, 2010). For many

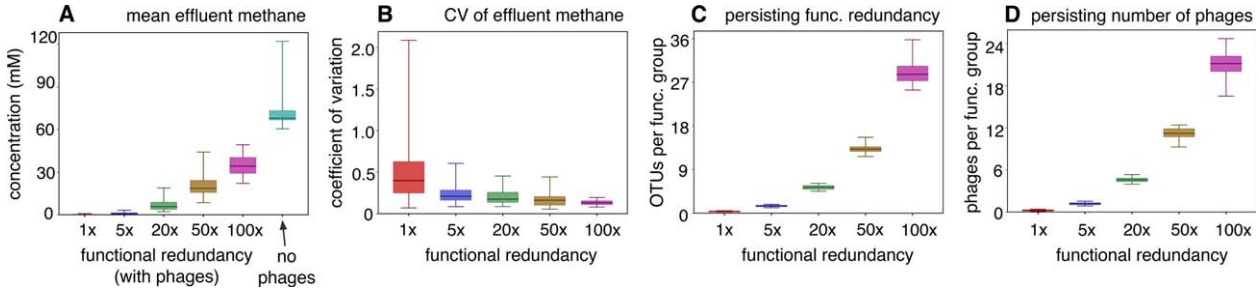

Fig. 3. Effects of functional redundancy on community performance.
(A) Temporal averages and (B) temporal coefficients of variation of effluent methane concentration, for various degrees of functional redundancy. In (A), also shown is the case without phages present (right-most box). (C) Number of OTUs occupying the top 99.9% of each functional group (counted in order of decreasing OTU abundance), averaged across functional groups and over time ('persisting functional redundancy'). (D) Number of persisting phages (i.e. with a density $>10^6\,L^{-1}$) per functional group, averaged across functional groups and over time. For example, at 50-fold functional redundancy, 99.9% of a functional group is accounted for by about 14 OTUs, and about 12 OTUs in each functional group have a specialist phage at density $>10^6\,L^{-1}$. In all figures, box plots represent the distribution across 100 random simulations. Whiskers span 95% percentiles around the median. For analogous analyses for lower N:C ratios in the inflow, see Supporting Information Fig. S2. [Colour figure can be viewed at wileyonlinelibrary.com]

phage-host pairs these fluctuations resemble classical predator-prey cycles, although most cycles are irregular in their phase and amplitude and reflect complex – potentially chaotic – dynamics (Supporting Information Fig. S1). In our model these complex fluctuations result from the coupling of phage-host cycles with the dynamics of the metabolic network, which mediates the interaction between distinct OTU populations. Complex – often chaotic – dynamics are common in systems composed of interacting oscillating components with distinct random frequencies (Grebogi *et al*., 1985). Such coupling of predator-prey dynamics with metabolic network dynamics may also explain irregular fluctuations sometimes observed in marine microbial communities at similar time scales (Needham *et al*., 2013; Needham and Fuhrman, 2016).

When averaged over time, predation by phages has detrimental effects on individual cell populations as well as on overall reaction rates. Especially at low functional redundancies ($\sim$1−20 fold), i.e. when only a few competing OTUs are available for performing a particular function, average methane production can drop down to just a small fraction ($\sim$1−30%) of the production that would typically be achieved in the absence of phages (Fig. 3A). Our model suggests that this reduction in performance can occur in at least two ways: First, increased cell mortality through cell lysis results in fewer cells that could consume a particular substrate before it is lost from the bioreactor. Second, because phage predation is biased towards dominant OTUs, it skews selection towards less competitive, i.e. metabolically less efficient OTUs within each functional group. This skewed selection leads to residual substrate concentrations that are higher than the equilibrium substrate concentrations that would establish in the exclusive presence of the top competitor. Due to the delays involved in either the recovery of populations or the opportunistic invasion by competitors, phages not only reduce the average metabolic throughput, but also induce fluctuations around that average (Fig. 3B). This may explain previously observed fluctuations of bioreactor performance that could not be fully explained using purely energetic and reaction-kinetic models (Smith and McCarty, 1990; Dumont *et al*., 2009; Louca and Doebeli, 2016).

Cell lysis could in principle increase microbial productivity through the release of organic material, contributing to a 'microbial loop' that enables recycling of limiting nutrients. Such productivity-enhancing effects of the viral shunt have been predicted for pelagic marine microbial food webs, where primary productivity is often limited by nitrogen or phosphorous (bottom-up control; Azam 1998; Jover *et al*., 2014; Weitz *et al*., 2015). While our model does include carbon and nitrogen recycling via cell lysis, cell lysis did not enhance community function. This apparent contrast to previous predictions may have multiple reasons: First, here we focussed on dissimilatory carbon flux rates (from glucose to methane), rather than on cell productivity. These flux rates were heavily affected by a reduction in cell density (due to 'top-down' control by phages), and unused reduced carbon was quickly lost through the bioreactor effluent. Second, most reduced carbon was used for energy gain rather than assimilation into biomass (as is common for anaerobic communities; McDuffie, 1991), and hence the contribution of carbon recycling to the overall reduced carbon pool is relatively small. Third, in the simulations discussed here (which resembled previous bioreactor experiments) nitrogen was not a limiting resource. When we repeated our simulations using a much lower molar N:C ratio (0.0075 instead of 0.075), nitrogen limitation severely affected methane production, both in the absence as well as presence of phages (bottom-up control; Supporting Information Fig. S2A). In those

cases, the negative effects of phages on community function (when compared with the case where phages were absent) became less severe, but they did not disappear entirely (Supporting Information Fig. S2). While nutrient recycling via viral lysis may have some positive effects on dissimilatory carbon fluxes (mitigating bottom-up limitation), in our model these effects are dominated by the detrimental effects of phages on cell populations (top-down limitation).

Functional redundancy promotes functional stability

When considering multiple degrees of functional redundancy, we find a clear trend towards higher as well as more stable overall methane production rates at elevated functional redundancies (Fig. 3A and B and Supporting Information Fig. S3B and D). This suggests that the opportunistic growth of functionally similar OTUs can mitigate the detrimental effects of phage predation on community function by filling underutilized metabolic niches, thereby increasing and stabilizing overall community function. The probability that an alternative OTU is able to quickly replace a collapsing competitor increases with functional redundancy, although even at a 100-fold functional redundancy methane production rates remained lower (i.e. at 50–60%) than those achieved in the absence of phages. Functional niche complementation is generally thought to promote a positive correlation between community richness and functional stability against external environmental perturbations (Tilman, 1996; Peterson *et al*., 1998; Briones and Raskin, 2003; Wittebolle *et al*., 2009). Our work suggests that functional complementation in microbial communities also partly mitigates the detrimental effects that intrinsically emerging (rather than externally driven) fluctuations can have on ecosystem functioning. This may explain the occasionally observed positive relationship between microbial species diversity and biochemical performance, particularly at low diversities, even in the absence of external perturbations (Griffiths *et al*., 1997; Wohl *et al*., 2004; Werner *et al*., 2011).

Phage predation has been previously hypothesized to stabilize bioreactor performance by preventing competitive exclusion between competing OTUs, thereby maintaining a high functional redundancy which, in turn, buffers the system against external perturbations (Shapiro and Kushmaro, 2011). Our analysis suggests that this interpretation of phages stabilizing community function need not always apply, because phage predation can actually reduce and destabilize community function when environmental conditions are constant. It is the availability of functional redundancy in the 'rare seed bank', which allows rare opportunists to counteract the destabilizing effects of phages. We note that this conclusion applies a priori mainly to systems where fluctuations in community structure and function caused by environmental fluctuations are much weaker than fluctuations caused by phage-host interactions. In that case, in the absence of phages competitive exclusion is predicted to lead to the persistence of a few OTUs with high substrate affinities and higher catabolic performance than in the presence of phages (Fig. 3D and H; Louca and Doebeli 2015b). In contrast, if environmental conditions fluctuate strongly, phages could in principle promote greater functional performance and stability by maintaining a rich repertoire of competitors adapted to current conditions, as hypothesized by Shapiro and Kushmaro (2011). This scenario remains largely speculative, because it is unclear how selection by phages at any moment in time couples with community responses to environmental fluctuations. In principle, predation by phages could select for organisms maladapted to the current environment due to tradeoffs between growth kinetics and defence mechanisms (Vage *et al*., 2013). Future extensions of the model incorporating varying environmental stochasticity (e.g. in temperature or pH), may help assess the relative benefits of phage-induced functional redundancy, compared with the detrimental effects of phages on the growth and metabolic activity of individual host populations.

At increased functional redundancy, our model predicts that functional community structure becomes more stable, although the extent of this stabilization depends on the functional groups considered (Fig. 4I–L). The stabilization of functional community structure is especially pronounced at the level of catabolic stages, i.e. when considering the proportions between all fermenters, all syntrophs and all methanogens (Fig. 4I). The coefficient of variation of the three catabolic stages drops from $\sim$1.3 (median value) in the absence of functional redundancy down to $\sim$0.2 at 100-fold functional redundancy. Since the three catabolic stages represent sequential and stoichiometrically coupled steps, their relative flux rates and productivities are subject to strong stabilizing forces (limitation of reaction rates by preceding steps, population growth in case of substrate accumulation). Our model thus provides an explicit explanation for the discrepancy between relatively steady functional community profiles (Fig. 4E) and highly variable taxonomic profiles (e.g. Fig. 2E–G and Supporting Information Fig. S3) often observed under constant environmental conditions (Dumont *et al*., 2009; Ofiţeru *et al*., 2010; Rodriguez-Brito *et al*., 2010; Louca *et al*., 2016a), and highlights the central role of functional redundancy combined with biotic interactions in promoting this discrepancy.

Within each catabolic stage, the proportions of individual functional groups (e.g. acetoclastic vs H_2/CO_2 methanogens) also stabilize at high functional redundancy, but the extent of stabilization depends on the specific set of reactions considered (Fig. 4J–L). For example, the proportions

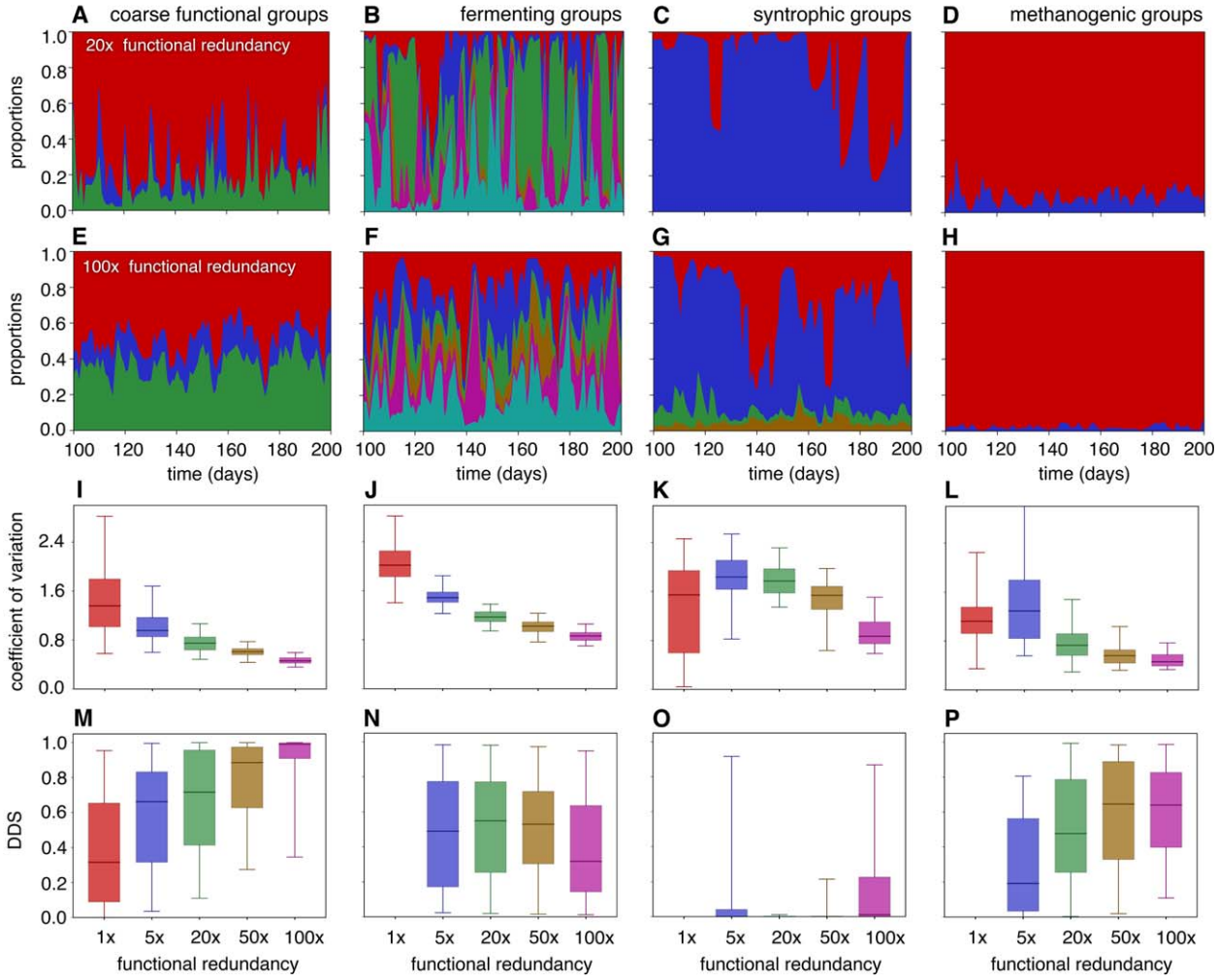

Fig. 4. Effects of functional redundancy on functional community structure. Row 1: Proportions of (A) cell densities grouped by catabolic stage (i.e. total fermenters vs total syntrophs vs total methanogens), (B) fermenting functional groups, (C) syntrophic functional groups and (D) methanogenic functional groups over time (one color per functional group), during a simulation at 20-fold functional redundancy. Each functional group consists of multiple OTUs (individual OTU populations not shown). Row 2: Similar to row 1, but for a simulation at 100-fold functional redundancy. For OTU proportions at the community level, and for methane concentrations in the effluent, see Supporting Information Fig. S3. Row 3: Coefficients of variation (CV) for the proportions of (I) cell densities grouped by catabolic stage, (J) fermenting functional groups, (K) syntrophic functional groups and (L) methanogenic functional groups, at various levels of functional redundancy. Row 4: Degree of dynamic stabilization (DDS) of functional group proportions, corresponding to I–L. Box plots (I–P) represent the distribution of CVs (I–L) and DDSs (M–P) across 100 random simulations; vertical bars indicate 95% percentiles. DDS was not calculated for 1× functional redundancy in N–P, as each functional group consists of only one OTU. For analogous analyses for lower N:C ratios in the inflow, see Supporting Information Fig. S4. [Colour figure can be viewed at wileyonlinelibrary.com]

between individual fermenting functional groups (A–F in Fig. 1) fluctuate substantially even at high functional redundancies (Fig. 4J), presumably because these groups represent strongly overlapping metabolic niches (they all ferment glucose). Fluctuations between these reactions, in turn, are predicted to drive comparably strong fluctuations in the proportions of syntrophic functional groups (Fig. 4K) specializing on different fermentation products (G–J in Fig. 1). Irregular transitions between alternative ('parallel') catabolic electron flows – congruently with stable overall catabolic performance – have been observed in previous experiments (Fernández *et al.*, 1999). In contrast, the proportions between the two methanogenic groups stabilize much faster. Hence, the stability of functional community structure depends on the precise definition and the subset of functional groups considered, because non-identical functional groups may be partly interchangeable in case of shared substrates or products (Peterson *et al.*, 1998). A distinction between parallel and sequential functional groups is particularly

crucial for 'branched' metabolic networks such as organic carbon catabolism, but may be less relevant for more sequential processes, such as nitrification (oxidizing ammonia to nitrite and then to nitrate).

Statistical averaging or dynamic stabilization?

As discussed above, a high functional redundancy can reverse the destabilizing effects that phage predation has on overall functional community structure and performance (Fig. 4A–L). Such stabilizing effects at increased species richness have been hypothesized in the past, based on the expectation that the effects of multiple fluctuating populations on broad community properties (such as total biomass or overall catabolic performance) ought to 'average' each other out (Tilman, 1996; Doak *et al.*, 1998). According to this interpretation, which assumes that populations fluctuate independently, the stabilization of broad community properties at elevated functional redundancy is a simple statistical necessity. In reality, however, populations are inevitably coupled due to competition for resources and metabolic interdependencies, and it is a priori unclear whether these interactions lead to stronger or weaker averaging effects (Tilman *et al.*, 1998). On the one hand, fluctuations in metabolite concentrations caused by changes in specific microbial populations will affect the growth of all functional groups consuming or producing these particular metabolites, and these effects will typically act in a similar direction on all members within a functional group. Such positive correlations in the response of competing populations to chemical perturbations would act against stabilization by averaging. On the other hand, the collapse of a particular population due to predation frees a metabolic niche that can be occupied by competing populations, and such a 'dynamic stabilization' would likely lead to a higher functional stability when compared with mere statistical averaging. A distinction between the two stabilizing mechanisms – statistical averaging versus dynamic stabilization – is key to understanding the effects of community interactions on overall functional stability.

To assess whether the functional stabilization observed in our simulations at high functional redundancy is a mere averaging effect, or is indeed dynamic, we compared the coefficients of variation of functional group abundances to a null model in which the entire time course of each OTU population is shifted in time by a distinct random lag. This null model resembles the hypothetical scenario in which populations fluctuate independently of one another (i.e. without interactions), while preserving point-to-point correlations within each population's time course. We defined the 'degree of dynamic stabilization' (DDS) in a particular simulation as the probability that the null model would lead to a higher coefficient of variation (averaged across catabolic stages or across functional groups) than observed. Hence, a DDS of 1.0 corresponds to full dynamic stabilization, that is, correlations between OTUs (mediated by metabolic interactions) tend to be such that functional groups maintain constant proportions. In contrast, a DDS of 0.0 means that interactions between OTUs act against statistical averaging. A DDS of 0.5 means that stabilization of functional group proportions can be explained purely by statistical averaging, and does not appear to be affected by community interactions. For example, if two OTUs oscillate in synchrony and in phase, then under the null model their phase difference would become randomly shifted. If these OTUs constituted a single functional group, then the overall abundance of that functional group would be less variable under the null model than originally observed (hence, DDS$<$0.5).

We found that the proportions between catabolic stages (fermenters vs syntrophs vs methanogens) exhibit a high DDS that approaches 1.0 at high degrees of functional redundancy (Fig. 4M), consistent with the interpretation that opportunistic competitors quickly replace collapsing populations. Within each catabolic stage, we found that the proportions of functional groups are rarely dynamically stabilized. For example, at 100-fold functional redundancy, the proportions between methanogenic groups exhibit a median DDS $\sim$0.6 (Fig. 4P), fermenting groups exhibit a median DDS $\sim$0.3 (Fig. 4N) and syntrophic groups exhibit a median DDS around zero (Fig. 4O). Hence, while in our model the proportions between catabolic stages tend to be stabilized by their sequential interdependencies (i.e. products of one stage are substrates for the next stage), this is not the case for functional group proportions within each catabolic stage. For example, functional groups consuming similar substrates (e.g. glucose in the case of fermenters) are highly interchangeable and hence their proportions are only weakly stabilized. The proportions of syntrophic groups, in turn, become dynamically destabilized, because they depend on alternative end-products of glucose catabolism.

Phages promote taxonomic and functional diversity

Classical competition theory predicts that at steady state only a single competitor can persist within a metabolic functional group that is limited by a single substrate, and this competitor is determined by its ability to survive at the lowest possible substrate concentration (Tilman, 1982; Louca and Doebeli, 2015b). In reality, however, microbial richness can be high even in simple engineered ecosystems, such as nitrifying bioreactors (Dumont *et al.*, 2009), methanogenic digesters (Godon *et al.*, 1997; Fernandez *et al.*, 2000), methanotrophic chemostats (Fernandez-Gonzalez *et al.*, 2016) or activated sludge (Kim *et al.*, 2013), where it can range from hundreds to thousands of OTUs. Such high richness is in apparent contradiction to the competitive exclusion principle. Mechanisms proposed

in the past to explain this contradiction include slow transient dynamics of competitive exclusion far from steady state (Louca and Doebeli, 2015b), negative frequency dependence through non-linear substrate dependencies (Stewart and Levin, 1973), externally driven fluctuations of resource availability or physical conditions (Stewart and Levin, 1973; Sommer, 1984), as well as phage-driven KTW dynamics (Thingstad and Lignell, 1997; Thingstad, 2000; Shapiro *et al*., 2010). Our work provides further support for KTW dynamics as an explanation for high OTU richness within metabolic functional groups, especially in the absence of obvious environmental fluctuations (Fernández *et al*., 1999; Ofiţeru *et al*., 2010; Shapiro *et al*., 2010; Fernandez-Gonzalez *et al*., 2016; Vanwonterghem *et al*., 2016). For example, in our simulations with 20-fold functional redundancy in the inoculum, at any point in time each functional group is occupied on average by 5–6 OTUs (Fig. 3C), each of which occasionally increases in relative abundance (Fig. 2F and G). Similarly, as mentioned earlier, the repeated disruption of reactions prevents the long-term mutual exclusion between alternative reactions limited by the same substrates, resulting in a 'parallelization' of catabolic fluxes. Notably, during most simulations multiple fermenting groups would contribute (occasionally or at all times) to the catabolism of glucose. Phage-induced catabolic parallelization can thus maintain functional diversity in addition to diversity within functional groups and may explain the co-occurrence of alternative intermediate products (e.g. multiple fatty acids) sometimes observed in methanogenic digesters (Xing *et al*., 1997; Hashsham *et al*., 2000; Vanwonterghem *et al*., 2014).

Neutral drift: An alternative explanation for OTU turnover?

Neutral population drift, i.e. stochastic fluctuations of population sizes due to random birth and death events within a community, has previously been suggested as an explanation for irregular OTU turnover within functional groups over time or between replicates, in sewage treatment plants (Sloan *et al*., 2006; Ofiţeru *et al*., 2010). In general, the importance of drift, when compared with deterministic processes such as competition and predation, is most relevant at small population sizes and/or when competing organisms are similar to each other (Lande *et al*., 2003). In typical aquatic systems, however, cell densities can be extremely high (e.g. $\sim 10^9$ cells $\cdot$ L^{-1} in lakes and up to 10^{13} cells $\cdot$ L^{-1} in bioreactors; Whitman *et al*., 1998; Krakat *et al*., 2010). Hence deterministic dynamics such as competitive exclusion between OTUs with even slight physiological differences are expected to dominate over demographic drift. Furthermore, even under purely neutral conditions, drift alone would only cause slow changes in population sizes because many random birth-death events would tend to average each other out, reducing the relative amplitude of fluctuations in population size. For example, even at population sizes as low as 10^4 cells, it would take a relatively rare OTU (10% proportion) on average 6923 days to become dominant (90% proportion) solely due to demographic drift (based on a neutral birth-death model with generation time of 1 day, Supplement S1). This back-of-the envelope calculation questions the plausibility of population drift as an explanation for OTU turnover in typical aquatic microbial communities, where time scales of turnover are in the order of days to months even under constant environmental conditions (Dumont *et al*., 2009; Ofiţeru *et al*., 2010; Rodriguez-Brito *et al*., 2010). In contrast, our model shows that deterministic ecological mechanisms can explain the OTU turnover within functional groups concurrent with a stable functional community structure, observed in realistic settings (Ofiţeru *et al*., 2010; Louca *et al*., 2016a).

Limitations

Although not modelled here, phage-host co-evolution could influence phage-host dynamics in natural systems (Middelboe *et al*., 2001; Shapiro *et al*., 2010; Gómez and Buckling, 2011; Weinberger *et al*., 2012). For example, the repeated emergence of new resistant strains could further destabilize population dynamics within functional groups. Rapid evolution of adaptive host resistance, for example via clustered regularly interspaced short palindromic repeats (CRISPRs; Andersson and Banfield, 2008), could buffer the impacts of viruses on overall ecosystem functioning (Lennon and Martiny, 2008). In addition, previous phage-host co-evolution models predicted that CRISPR immunity may induce host and phage diversification (Childs *et al*., 2012), although subsequent models suggested a rather modest contribution of CRISPR to the ecology of bacteria and phage (Levin *et al*., 2013). Our work suggests that deterministic ecological dynamics are sufficient to explain the succession of OTUs often observed during constant community function. In fact, Shapiro *et al*. (2010) observed rapid succession between distantly related OTUs and their associated phages in a bioreactor, suggesting that replacement by non-related competitors – rather than adaptive evolution of resistance – was indeed the main mode of host succession.

We note that the destabilizing role of phage predation and the stabilizing role of functional redundancy, as predicted by our model, rely on the assumption that lytic phages are specialized on single host populations (a prerequisite for KTW dynamics). High host specificities of phage infectivity (e.g. at the strain, species or genus level) are generally considered to be the rule (Holmfeldt *et al*., 2007; Paez-Espino *et al*., 2016), however deviations from this pattern also exist (Sullivan *et al*., 2003; Shapiro and Kushmaro, 2011; Paez-Espino

et al., 2016). For example, both modularity (i.e. preferential cross-infection of bacteria and phages within the same groups) as well as nestedness (i.e. a hierarchy of infectivity among phages and resistance among hosts) are repeatedly observed in phage-host interaction networks (Flores *et al*., 2011; Weitz *et al*., 2013). Hence, while specialist phage-host pairs may be abundant in a community, generalist phages or hosts susceptible to more than one phage may also be present. The effective functional redundancy in the community may thus be lower than the actual number of bacterial and archaeal strains, and the function-enhancing effects of increased functional redundancy may be less pronounced than reported here. Previous work showed that predation by generalist protist grazers can severely reduce community function (Thingstad and Lignell, 1997; Thomas *et al*., 2011; Johnke *et al*., 2014), although recent models suggest that nutrient recycling via cell lysis by generalist phages may increase primary productivity in the ocean (Weitz *et al*., 2015). Further, phages infecting distantly related hosts may promote mutual exclusion between functionally dissimilar populations due to apparent competition (Chase *et al*., 2002). The effects of phages on real communities are likely a combination of the effects predicted here (e.g. taxonomic turnover over time despite constant function) and the effects previously predicted for generalist predators (e.g. reduction of host biomass). Additional work is needed to asses how apparent competition between functionally dissimilar hosts (due to generalist phages) interacts with a maintenance of diversity within functional groups due to specialist phages, and how the coexistence of generalist and specialist phages affects metabolic network dynamics. To answer these questions, our model could be extended to a network context [e.g. Jover *et al*., 2013], where each phage can infect one or multiple hosts and vice versa, based on realistic infection networks (Flores *et al*., 2011; Weitz *et al*., 2013).

Lysogenic phage strategies, not considered here, likely have less severe effects on host populations and metabolic throughput than predicted by our model. For example, recent findings suggest that phages may be switching from lytic to lysogenic during high host abundances, a behaviour termed 'piggy-backing the winner' (Knowles *et al*., 2016), and this switching may dampen oscillations in host abundances. Hence, in environments characterized by lysogenic – rather than lytic – phage-host interactions (as may be the case for the human gut, Reyes *et al*., 2012), KTW dynamics will be less pronounced and hence microbial communities may be more stable in terms of their taxonomic composition.

Conclusions

Microbial communities can display strong taxonomic variation across space and time even under similar environmental conditions, while exhibiting relatively constant functional community structure (Ofiţeru *et al*., 2010; Rodriguez-Brito *et al*., 2010; Fernandez-Gonzalez *et al*., 2016; Louca *et al*., 2016a). In a recent study, environmental conditions strongly predicted the distribution of metabolic functional groups across the world's ocean, but only poorly predicted the taxonomic composition within individual functional groups (Louca *et al*., 2016b). Louca *et al*. (2016a) showed that OTUs within individual functional groups displayed non-random phylogenetic relationships and non-random co-occurrence patterns, and concluded that OTU turnover between samples was at least partly caused by mechanisms exhibiting a phylogenetic signal, such as biotic interactions. These findings suggest a paradigm for microbial ecology in which the functional structure and the taxonomic composition within functional groups constitute two separate facets of community composition, with the former being driven by stoichiometric and energetic environmental constraints, while the latter is heavily influenced by biotic interactions that are not directly related to metabolism. Our model provides further support for such an interpretation by explicitly demonstrating how – and under which conditions – predation by specialist phages can drive OTU turnover while maintaining constant functional community structure and metabolic performance. Prolonged transients of competitive exclusion may also lead to slow OTU turnover within functional groups, especially following environmental perturbation (Louca and Doebeli, 2015b), although the detection of correlated OTU and phage succession in bioreactors provides additional evidence for KTW dynamics in these systems (Rodriguez-Brito *et al*., 2010; Shapiro *et al*., 2010). Overall, experimental evidence for phage-driven KTW dynamics is still limited (Middelboe *et al*., 2001; Ovreas *et al*., 2003; Rodriguez-Valera *et al*., 2009; Vos *et al*., 2009; Rodriguez-Brito *et al*., 2010; Shapiro *et al*., 2010), mostly due to the technical difficulties involved in virome profiling and in linking particular phages to their specific hosts in natural ecosystems. Nevertheless, many ecosystems, including the open ocean (Suttle, 2007) or the human gut (Reyes *et al*., 2012), exhibit high phage densities, and it is possible that phages also contribute to a decoupling between taxonomic and functional community structure in these environments (Raes *et al*., 2011; Frossard *et al*., 2012; Louca *et al*., 2016a,b).

The decoupling between functional and taxonomic community structure, especially at high functional redundancy, has important implications for the interpretation of microbial biogeographical patterns, because variation in taxonomy need not imply differences in community function. Reciprocally, environmental constraints determining community function may only poorly explain the distribution of individual taxa. If phage-induced KTW dynamics or, more generally, biotic interactions strongly shape the taxonomic variation within functional groups, as suggested by this

and previous work, then the aspiration of accurate microbial species distribution models (Strom, 2008; Larsen *et al.*, 2012) may turn out to be a Sisyphean struggle. Disentangling the functional variation from the taxonomic variation within functional groups is thus an important prerequisite for a predictive microbial ecology.

Experimental procedures

Model overview

Our model describes the population dynamics of multiple bacterial and archaeal operational taxonomic units (OTUs), their reaction kinetics, the population dynamics of multiple phage populations, as well as extracellular metabolite concentrations in a flow-through bioreactor. Here, an 'OTU' represents a clade that is specialized on a specific metabolic function (e.g. acetoclastic methanogenesis), and that is preyed upon by a single specialist phage population. Hence, an OTU represents a taxonomic group that is sufficiently narrow so that reaction kinetics are similar across members, and sufficiently broad so that different OTUs have different specialist phages. An OTU in our model is roughly analogous to a single prokaryotic species or strain (Holmfeldt *et al.*, 2007; Paez-Espino *et al.*, 2016) (but see our discussion in the main text).

The bioreactor model largely resembles the setup used in previous experiments (Xing *et al.*, 1997; Fernández *et al.*, 1999). The bioreactor's interior is assumed to be well mixed and anaerobic. Glucose (for catabolism and biosynthesis) and ammonium (for biosynthesis) are supplied continuously to the bioreactor as part of a sterile steady inflow, which is balanced by an equivalent outflow that removes residual substrates, metabolic by-products as well as cells and free phage particles at a constant dilution rate. Cell death leads to an additional flux of dissolved organic carbon (in the form of glucose) as well as ammonium into the bioreactor. pH and temperature are assumed to be maintained at constant levels, in analogy to previous bioreactor experiments (Wittebolle *et al.*, 2008; Dumont *et al.*, 2009; Vanwonterghem *et al.*, 2014; 2016). We note that in experiments where pH was not externally controlled, functional stability typically coincided with a stability of pH, presumably as a balance between microbial and abiotic chemical processes (Fernández *et al.*, 1999; Ofiţeru *et al.*, 2010).

The mathematical model structure, described in detail below, is relatively standard. A comprehensive view of the phage-microbe components can be found in the recent monograph by Joshua Weitz (Weitz, 2015).

Reaction rates and metabolite dynamics

The model considers a total of 12 reactions ('functional groups'), driving the stepwise catabolism of glucose all the way to the production of methane and CO_2 (see Supporting Information Table S1 for a list of reactions and Fig. 1 for a schematic overview). Each OTU is associated with a single metabolic reaction, such as fermentation of glucose to ethanol or acetoclastic methanogenesis, but each reaction, or function, may be performed by multiple competing OTUs.

Each reaction couples the uptake of one or more substrates to the export of one or more products into the extracellular medium and the assimilation of substrates into cell biomass, thereby affecting the concentrations of dissolved metabolites in the bioreactor. Specifically, the concentration of the m-th metabolite, C_m, changes according to the differential equation

$$\frac{dC_m}{dt} = D(C_m^o - C_m) + \sum_r (S_{mr} - A_{mr} Y_r) \sum_{s \in J_r} N_s H_s + F_m, \quad (1)$$

where J_r is the set of OTUs performing reaction r, N_s is the cell concentration of OTU s, H_s is the cell-specific rate of the reaction performed by OTU s (mol per time per cell), D is the dilution rate, C_m^o is the metabolite's concentration in the inflow (zero for all metabolites except glucose and ammonium), A_{mr} is the amount of metabolite m assimilated into biomass during reaction r (mol assimilated per gram dry biomass), Y_r is the biomass yield of reaction r (gram dry biomass per mol), F_m accounts for additional metabolite influx due to cell death (specified below), and S_{mr} is the stoichiometric coefficient of metabolite m in reaction r. For example, for glucose fermentation to ethanol (reaction 'A' in Fig. 1),

$$C_6H_{12}O_6 \rightarrow 2\,CH_3CH_2OH + 2\,CO_2, \quad (2)$$

the stoichiometric coefficients of glucose, ethanol and CO_2 are -1, $+2$ and $+2$ respectively.

For all functional groups except for H_2/CO_2 methanogenesis (reactions A–L in Fig. 1), the corresponding electron donor (glucose, ethanol, lactate, propionate or butyrate) is assumed to serve as the sole carbon source for biosynthesis, whereas for H_2/CO_2 methanogenesis CO_2 is assumed to serve as sole carbon source. For all functional groups, ammonium is assumed to serve as nitrogen source for biosynthesis. For example, for glucose fermentation to ethanol, all assimilation factors $A_{m,\mathrm{A}}$ are zero except for glucose and ammonium:

$$A_{\mathrm{gluc,A}} = \frac{1}{6} W_{\mathrm{C}}, \quad A_{\mathrm{amm,A}} = W_{\mathrm{N}}, \quad (3)$$

where W_{C} is the amount of carbon assimilated per biomass (0.0375 mol-C per gram dry biomass) and W_{N} is the amount of nitrogen assimilated per biomass (0.00932 mol-N per gram dry biomass), as reported for exponentially growing *Escherichia coli* cells (Fagerbakke *et al.*, 1996).

The cell-specific reaction rate H_s is assumed to be limited by 3 factors: (a) the availability of the electron donor substrate (such as glucose in the case of fermenters, or H_2 in the case of H_2/CO_2 methanogens), (b) the availability of ammonium for assimilation and (c) the minimum amount of energy required to maintain the cell's membrane potential (LaRowe *et al.*, 2012). In particular, nutrient limitation of metabolic rate is determined by the most limiting nutrient (the electron donor or nitrogen) (Follows *et al.*, 2007). Specifically, for any OTU s performing reaction r we set H_s to the minimum of $h_s \cdot \Phi_r$ and $J_{\mathrm{amm}}/(A_{\mathrm{amm,r}} Y_r)$, where J_{amm} is the maximum possible cell-specific ammonium uptake rate (mol-N per cell per time, limited by extracellular ammonium diffusion rates; Shaw *et al.*, 2015), h_s accounts for the dependence on substrate availability according to classical Monod kinetics (Jin *et al.*, 2013) and Φ_r is a thermodynamic potential factor for the reaction

(LaRowe *et al.*, 2012), accounting for reduced reaction rates near thermodynamic equilibrium:

$$h_s = \frac{V_s C}{C + K_s}, \tag{4}$$

$$J_{\text{amm}} = 4\pi R_c D_{\text{amm}} C_{\text{amm}}, \tag{5}$$

$$\Phi_r = \left[\exp\left(\frac{\Delta G_r + F \cdot \Delta\Psi}{R_g T}\right) + 1\right]^{-1}. \tag{6}$$

Here, K_s is the half-saturation concentration of the limiting substrate (specific to OTU *s*), C is the substrate concentration, V_s is the maximum cell-specific reaction rate (specific to OTU *s*), D_{amm} is the ammonium molecular diffusion coefficient, R_c is the cell radius, $R_g = 8.314\,\text{J}\cdot\text{K}\cdot\text{mol}^{-1}$ is the molar gas constant, T is the temperature in Kelvin, $\Delta\Psi$ is the electric potential across the cell membrane, $F = 96.485\,\text{kJ}\cdot\text{V}^{-1}\cdot\text{mol}^{-1}$ is the Faraday constant and ΔG_r is the Gibbs free energy of the reaction per electron transferred. Note that ΔG_r is given by

$$\Delta G_r = \frac{1}{\gamma_r}\left[\Delta G_r^o + R_g T \ln Q_r\right], \tag{7}$$

where ΔG_r^o is the standard Gibbs free energy of the reaction (kJ per mol e-donor), γ_r is the number of transferred electrons (mol e^- per mol e-donor, overview in Supporting Information Table S1), and

$$Q_r = \prod_m C_m^{S_{mr}} \tag{8}$$

is the reaction quotient.

We mention that we were mainly interested in the possible effects of N limitation on C fluxes when N:C molar ratios are low, and not on N fluxes at higher N concentrations per se. Hence, for simplicity, and to minimize dependency on additional parameters (e.g. half-saturation constants), in our model maximum ammonium uptake rates follow 1st order kinetics, i.e. they are proportional to ammonium concentrations (Eq. (5)). That said, we emphasize that ammonium uptake at any moment in time is stoichiometrically coupled to biosynthesis, and hence actual ammonium uptake rates saturate at excessive ammonium concentrations when the electron donor becomes limiting (thus resembling saturating, e.g. Monod, uptake kinetics).

Cell and phage population dynamics

For each OTU *s* performing some reaction *r*, the total cell production rate is assumed to be proportional to the total rate of its catalyzed reaction, $H_s N_s$, multiplied by some constant biomass yield factor, Y_r, and divided by the dry cell mass, m_s. We note that using constant yield factors to describe microbial growth rates is only an approximation (McDuffie, 1991). Nevertheless, our model successfully captures key aspects of microbial metabolic networks, including stoichiometric balancing between metabolic pathways, substrate limitation and a halt of reaction rates near thermodynamic equilibrium or when reactions become endergonic (i.e. $H_s \approx 0$ when $\Delta G_r \lesssim 0$; LaRowe *et al.*, 2012).

Each OTU *s* is associated with a single specialist lytic phage population, which comprises free phage particles as well as phages that have infected a host cell. The model keeps track of the infected portion, N_s^{i}, and the uninfected portion, N_s^{u}, of each cell population. The rate at which uninfected cells become infected is proportional to the total number of free phage particles (P_s) and to the total number of uninfected cells (Ellis and Delbrück, 1939), multiplied by some proportionality constant (β_s) that accounts for the rate at which phages 'scan' the medium via passive diffusion (volume clearance rate) as well as the probability that an encounter with a cell would lead to infection (Middelboe *et al.*, 2001). All infected cells are assumed to eventually undergo lysis, releasing new phage particles into the bioreactor (Shapiro and Kushmaro, 2011). Lysogeny is not considered in the model. The loss of uninfected cells is assumed to be driven by hydraulic dilution, and is hence described by an exponential decay rate D. In addition to hydraulic dilution, infected cells suffer from an elevated mortality rate, μ_s, which is equivalent to the inverse of the time lag between infection and cell lysis (latent period). Hence, uninfected and infected cell concentrations change according to the differential equations

$$\frac{dN_s^{\text{u}}}{dt} = \frac{Y_r}{m_s} N_s^{\text{u}} H_s - D N_s^{\text{u}} - \beta_s P_s N_s^{\text{u}}, \tag{9}$$

$$\frac{dN_s^{\text{i}}}{dt} = \beta_s P_s N_s^{\text{u}} - D N_s^{\text{i}} - \mu_s N_s^{\text{i}}. \tag{10}$$

Here, m_s is the dry cell mass for OTU *s*.

Phage-induced cell lysis leads to the release of new free phage particles. The adsorption of phage particles by already infected cells has no further effect on the cell burst size or time lag of cell lysis (Ellis and Delbrück, 1939), but contributes to the removal of phage particles from the bioreactor. Phage particles that fail to infect any cells are assumed to decay naturally (i.e. become inactivated or destroyed) (Suttle, 1994) or to eventually get flushed out of the bioreactor. Hence, the concentration of infectious phage particles associated with OTU *s* satisfies the differential equation

$$\frac{dP_s}{dt} = \nu_s \mu_s N_s^{\text{i}} - \beta_s P_s (N_s^{\text{u}} + N_s^{\text{i}}) - (D + \delta_s) P_s, \tag{11}$$

where ν_s is the average number of phage particles released per lysed cell (burst size), and δ_s is the phage inactivation rate.

As mentioned in the previous section, cell lysis results in the release of organic carbon (in the form of glucose) and ammonium into the bioreactor, available for subsequent catabolism and assimilation. Hence, the flux terms F_m (Eq. (1)) are zero for all metabolites *m* except for glucose and ammonium:

$$F_{\text{gluc.}} = \frac{W_{\text{C}}}{6} \sum_s \mu_s N_s^{\text{i}} m_s, \tag{12}$$

$$F_{\text{NH}_4^+} = W_{\text{N}} \sum_s \mu_s N_s^{\text{i}} m_s. \tag{13}$$

Parameterization and simulations

Model parameters were either fixed at values obtained from the literature, or chosen randomly and uniformly within an

interval around values obtained from the literature (overview in Supporting Information Table S2), following a similar approach by Follows *et al.* (2007). In particular, for each OTU the reaction-kinetic parameters (V_s and K_s; Eq. (4)) as well as parameters describing phage-host interactions (β_s, ν_s and μ_s; Eqs. (9–11)) were chosen randomly for each OTU. To account for tradeoffs between the kinetic parameters K_s and V_s (Follows *et al.*, 2007), as well as for tradeoffs between defence against phages and growth rates, for each OTU we set $V_s = V_s^o \kappa_s \lambda_s$, $K_s = K_s^o \kappa_s/(1-\kappa_s)$ and $\beta_s = \beta_s^o \lambda_s$, where V_s^o, K_s^o and β_s^o are chosen randomly as in Supporting Information Table S2, and κ_s, λ_s are chosen randomly and uniformly between 0 and 1. The parameter κ_s mediates the tradeoff between the affinity (i.e. the ratio V_s/K_s) and the maximum cell-specific reaction rate (V_s), as recommended by Smith *et al.* (2009), and consistent with suggestions by Aksnes and Cao (2011) that affinity – rather than half-saturation concentration – is an inherent biological trait. Similarly, the parameter λ_s mediates the tradeoff between defence and growth, following a similar approach by Vage *et al.* (2013). Yield factors were taken directly from Roden and Jin (2011, Supporting Information Table S2 therein) or, if not available, were estimated based on the reaction's standard Gibbs free energy (ΔG_r^o) and the regression formula provided by Roden and Jin (2011).

The glucose concentration in the inflow (C^o_{gluc}) was set to $1\,\text{g}\cdot\text{L}^{-1}$. This concentration is between typical dissolved organic carbon concentrations in natural methanogenic environments (Jones *et al.*, 1995; Wand *et al.*, 2006) on the one hand, and typical bioreactor feeds (Xing *et al.*, 1997; Fernández *et al.*, 1999) on the other hand. The choice of glucose input (within ranges spanning natural and bioreactor systems) did not influence our overall conclusions.

The ammonium concentration in the inflow (C^o_{amm}) was set to $6\alpha C^o_{\text{gluc}}$, where α is the molar nitrogen:carbon (N:C) ratio. Unless otherwise mentioned, for α we considered the value 0.075, which is the ratio used in experiments by Xing *et al.* (1997) and Fernández *et al.* (1999), and is also comparable to values in other similar experiments (Vanwonterghem *et al.*, 2014; 2016). We note that this ratio is about half of the Redfield N:C ratio (16:106 = 0.15). Considering that in anaerobic digesters the bulk of reduced carbon is catabolized for energy rather than assimilated (McDuffie, 1991), N was unlikely a limiting resource in the aforementioned experiments. Here, to explore the interaction between nitrogen limitation and the release of nitrogen by viral lysis in more oligotrophic environments (Rosenberg *et al.*, 2010), we performed additional simulations using a much lower N:C ratio of 0.0075.

Apart from the random parameter choices described here, no model selection/constraining was done. In particular, we did not make any a priori assumptions as to which phages or OTUs persist in the long term. Instead, for each simulation we allowed the system's dynamics determine which phages and OTUs persisted. We note that this is also the approach taken by Follows *et al.* (2007). The number of OTUs and phages persisting within each functional group are shown in Fig. 3C and D.

The differential equations (1), (9), (10) and (11) describe a high-dimensional deterministic dynamical system of $3S+M$ variables, where S is the number of OTUs and M is the number of considered metabolites. Numerical simulations of this system were performed using MCM 1.7 (Louca and Doebeli, 2015a), an open source software for modelling microbial communities. MCM is available at: http://www.zoology.ubc.ca/MCM

Statistical analysis

To quantify the metabolic performance of the community (in terms of methane production), for each simulation we calculated the average effluent methane concentration over time. To quantify the variation in metabolic performance we calculated the coefficient of variation (CV, i.e. the standard deviation divided by the average) of effluent methane concentration over time. Note that for each simulation the average methane concentration and its CV were different because several model parameters were chosen randomly. For each degree of functional redundancy, we used 50 simulations to estimate the distribution of average methane concentrations and their CVs (box-plots in Fig. 3A and B).

To quantify the variation in functional community structure across time during any particular simulation, we calculated the CVs of functional group proportions and averaged these over all considered functional groups. For example, to quantify the variation of the 3 catabolic stages (all fermenters vs all syntrophs vs all methanogens) we considered the average of (a) the CV of the fraction of fermenters, (b) the CV of the fraction of syntrophs and (c) the CV of the fraction of methanogens in the community. Similarly, to quantify the variation of methanogenic functional groups we considered the average of (a) the CV of the fraction of acetoclastic methanogens and (b) the CV of the fraction of H_2/CO_2 methanogens. Note that CVs were different for each simulation, because several model parameters were chosen randomly. For each degree of functional redundancy, we used 50 simulations to estimate the distribution of CVs (box-plots in Fig. 4I–L).

As mentioned earlier, to distinguish between statistical averaging and dynamic stabilization we compared the CVs of functional group proportions to a null model in which OTU populations fluctuated independently. Specifically, for each simulation the null model cyclically shifted the time series of each OTU by a random time step, resulting in hypothetical community trajectories in which each OTU population fluctuates at a random phase lag when compared with other OTUs. The shifted time series of all OTUs within each functional group were then summed to calculate the hypothetical corresponding abundance of the functional group. For each simulation this was done 1000 times, yielding a distribution of random CVs generated by the null model. The 'degree of dynamic stabilization' (DDS) of a single simulation was then defined as the fraction of random CVs that were above the actual CV of the simulation. For each degree of functional redundancy, we used 50 simulations to estimate the distribution of DDSs (box-plots in Fig. 4M–P).

All simulations were ran for a period of 200 days. All statistics were performed based on days 50–200, in order to avoid any transients during 'startup phase'.

Acknowledgements

We thank Jan Finke, Sarah P. Otto and Steven J. Hallam for comments on our manuscript. S.L. acknowledges the financial support of the Department of Mathematics and the Faculty of

Graduate Studies, University of British Columbia. S.L. and M.D. acknowledge the support of NSERC.

Competing interests

The authors declare that they have no competing financial interests.

Additional information

Correspondence and requests for materials should be addressed to S.L. Supporting figures and tables, cited in the text, are provided as Supplementary Material.

References

Aksnes, D.L., and Cao, F.J. (2011) Inherent and apparent traits in microbial nutrient uptake. *Mar Ecol Prog Ser* **440:** 41–51.

Andersson, A.F., and Banfield, J.F. (2008) Virus population dynamics and acquired virus resistance in natural microbial communities. *Science* **320:** 1047–1050.

Azam, F. (1998) Microbial control of oceanic carbon flux: The plot thickens. *Science* **280:** 694–696.

Barr, J.J., Slater, F.R., Fukushima, T., and Bond, P.L. (2010) Evidence for bacteriophage activity causing community and performance changes in a phosphorus-removal activated sludge. *FEMS Microbiol Ecol* **74:** 631–642.

Briones, A., and Raskin, L. (2003) Diversity and dynamics of microbial communities in engineered environments and their implications for process stability. *Curr Opin Biotechnol* **14:** 270–276.

Chase, J.M., Abrams, P.A., Grover, J.P., Diehl, S., Chesson, P., Holt, R.D., *et al.* (2002) The interaction between predation and competition: a review and synthesis. *Ecol Lett* **5:** 302–315.

Childs, L.M., Held, N.L., Young, M.J., Whitaker, R.J., and Weitz, J.S. (2012) Multiscale model of CRISPR-induced coevolutionary dynamics: diversification at the interface of Lamarck and Darwin. *Evolution* **66:** 2015–2029.

Conrad, R. (1999) Contribution of hydrogen to methane production and control of hydrogen concentrations in methanogenic soils and sediments. *FEMS Microbiol Ecol* **28:** 193–202.

Doak, D.F., Bigger, D., Harding, E., Marvier, M., O'malley, R., and Thomson, D. (1998) The statistical inevitability of stability-diversity relationships in community ecology. *Am Nat* **151:** 264–276.

Dumont, M., Harmand, J., Rapaport, A., and Godon, J.J. (2009) Towards functional molecular fingerprints. *Environ Microbiol* **11:** 1717–1727.

Ellis, E.L., and Delbrück, M. (1939) The growth of bacteriophage. *J Gen Physiol* **22:** 365–384.

Fagerbakke, K., Heldal, M., and Norland, S. (1996) Content of carbon, nitrogen, oxygen, sulfur and phosphorus in native aquatic and cultured bacteria. *Aquat Microb Ecol* **10:** 15–27.

Fernández, A., Huang, S., Seston, S., Xing, J., Hickey, R., Criddle, C., *et al.* (1999) How stable is stable? Function versus community composition. *Appl Environ Microbiol* **65:** 3697–3704.

Fernandez, A.S., Hashsham, S.A., Dollhopf, S.L., Raskin, L., Glagoleva, O., Dazzo, F.B., *et al.* (2000) Flexible community structure correlates with stable community function in methanogenic bioreactor communities perturbed by glucose. *Appl Environ Microbiol* **66:** 4058–4067.

Fernandez-Gonzalez, N., Huber, J.A., and Vallino, J.J. (2016) Microbial communities are well adapted to disturbances in energy input. *mSystems* **1:** e00117–16.

Flores, C.O., Meyer, J.R., Valverde, S., Farr, L., and Weitz, J.S. (2011) Statistical structure of host–phage interactions. *Proc Natl Acad Sci USA* **108:** E288–E297.

Follows, M.J., Dutkiewicz, S., Grant, S., and Chisholm, S.W. (2007) Emergent biogeography of microbial communities in a model ocean. *Science* **315:** 1843–1846.

Frossard, A., Gerull, L., Mutz, M., and Gessner, M.O. (2012) Disconnect of microbial structure and function: enzyme activities and bacterial communities in nascent stream corridors. *ISME J* **6:** 680–691.

Fuhrman, J.A. (1999) Marine viruses and their biogeochemical and ecological effects. *Nature* **399:** 541–548.

Godon, J.J., Zumstein, E., Dabert, P., Habouzit, F., and Moletta, R. (1997) Molecular microbial diversity of an anaerobic digestor as determined by small-subunit rDNA sequence analysis. *Appl Environ Microbiol* **63:** 2802–2813.

Gómez, P., and Buckling, A. (2011) Bacteria-phage antagonistic coevolution in soil. *Science* **332:** 106–109.

Grebogi, C., Ott, E., and Yorke, J.A. (1985) Attractors on an n-torus: Quasiperiodicity versus chaos. *Phys D* **15:** 354–373.

Griffiths, B.S., Ritz, K., and Wheatley, R.E. (1997) Relationship between functional diversity and genetic diversity in complex microbial communities. In *Microbial communities: functional versus structural approaches*. Insam, H., and Rangger, A. (eds.). Berlin, Heidelberg: Springer Berlin Heidelberg, pp. 1–9.

Guidi, L., Chaffron, S., Bittner, L., Eveillard, D., Larhlimi, A., Roux, S., *et al.* (2016) Plankton networks driving carbon export in the oligotrophic ocean. *Nature* **532:** 465–470.

Hashsham, S.A., Fernandez, A.S., Dollhopf, S.L., Dazzo, F.B., Hickey, R.F., Tiedje, J.M., *et al.* (2000) Parallel processing of substrate correlates with greater functional stability in methanogenic bioreactor communities perturbed by glucose. *Appl Environ Microbiol* **66:** 4050–4057.

Holmfeldt, K., Middelboe, M., Nybroe, O., and Riemann, L. (2007) Large variabilities in host strain susceptibility and phage host range govern interactions between lytic marine phages and their *Flavobacterium* hosts. *Appl Environ Microbiol* **73:** 6730–6739.

Jin, Q., Roden, E.E., and Giska, J.R. (2013) Geomicrobial kinetics: Extrapolating laboratory studies to natural environments. *Geomicrobiol J* **30:** 173–185.

Johnke, J., Cohen, Y., de Leeuw, M., Kushmaro, A., Jurkevitch, E., and Chatzinotas, A. (2014) Multiple micropredators controlling bacterial communities in the environment. *Curr Opin Biotechnol* **27:** 185–190.

Jones, J.B., Holmes, R.M., Fisher, S.G., Grimm, N.B., and Greene, D.M. (1995) Methanogenesis in Arizona, USA dryland streams. *Biogeochemistry* **31:** 155–173.

Jover, L.F., Cortez, M.H., and Weitz, J.S. (2013) Mechanisms of multi-strain coexistence in host–phage systems with nested infection networks. *J Theor Biol* **332:** 65–77.

Jover, L.F., Effler, T.C., Buchan, A., Wilhelm, S.W., and Weitz, J.S. (2014) The elemental composition of virus particles: implications for marine biogeochemical cycles. *Nat Rev Microbiol* **12:** 519–528.

Kim, T.S., Jeong, J.Y., Wells, G., and Park, H.D. (2013) General and rare bacterial taxa demonstrating different temporal dynamic patterns in an activated sludge bioreactor. *Appl Microbiol Biotechnol* **97:** 1755–1765.

Knowles, B., Silveira, C., Bailey, B., Barott, K., Cantu, V., Cobián-Güemes, A., *et al.* (2016) Lytic to temperate switching of viral communities. *Nature* **531:** 466–470.

Krakat, N., Westphal, A., Schmidt, S., and Scherer, P. (2010) Anaerobic digestion of renewable biomass: Thermophilic temperature governs methanogen population dynamics. *Appl Environ Microbiol* **76:** 1842–1850.

Lande, R., Engen, S., and Sæther, B. (2003) *Stochastic Population Dynamics in Ecology and Conservation. Oxford Series in Ecology and Evolution*. Oxford University Press. 222 pages. ISBN-10: 0198525257. Oxford, UK.

LaRowe, D.E., Dale, A.W., Amend, J.P., and Van Cappellen, P. (2012) Thermodynamic limitations on microbially catalyzed reaction rates. *Geochim Cosmochim Acta* **90:** 96–109.

Larsen, P., Hamada, Y., and Gilbert, J. (2012) Modeling microbial communities: Current, developing, and future technologies for predicting microbial community interaction. *J Biotechnol* **160:** 17–24.

Lennon, J.T., and Martiny, J.B.H. (2008) Rapid evolution buffers ecosystem impacts of viruses in a microbial food web. *Ecol Lett* **11:** 1178–1188.

Levin, B.R., Moineau, S., Bushman, M., and Barrangou, R. (2013) The population and evolutionary dynamics of phage and bacteria with CRISPR–mediated immunity. *PLoS Genet* **9:** e1003312.

Louca, S., and Doebeli, M. (2015a) Calibration and analysis of genome-based models for microbial ecology. *eLife* **4:** e08208.

Louca, S., and Doebeli, M. (2015b) Transient dynamics of competitive exclusion in microbial communities. *Environ Microbiol* **18:** 1863–1874.

Louca, S., and Doebeli, M. (2016) Reaction-centric modeling of microbial ecosystems. *Ecol Model* **335:** 74–86.

Louca, S., Jacques, S.M.S., Pires, A.P.F., Leal, J.S., Srivastava, D.S., Parfrey, L.W., *et al.* (2016a) High taxonomic variability despite stable functional structure across microbial communities. *Nat Ecol Evol* **1:** 0015.

Louca, S., Parfrey, L.W., and Doebeli, M. (2016b) Decoupling function and taxonomy in the global ocean microbiome. *Science* **353:** 1272–1277.

McDuffie, N.G. (1991) *Bioreactor Design Fundamentals*. USA: Butterworth-Heinemann.

Middelboe, M., Hagström, A., Blackburn, N., Sinn, B., Fischer, U., Borch, N., *et al.* (2001) Effects of bacteriophages on the population dynamics of four strains of pelagic marine bacteria. *Microb Ecol* **42:** 395–406.

Mladenovska, Z., and Ahring, B.K. (2000) Growth kinetics of thermophilic *Methanosarcina* spp. isolated from full-scale biogas plants treating animal manures. *FEMS Microbiol Ecol* **31:** 225–229.

Needham, D.M., Chow, C.E.T., Cram, J.A., Sachdeva, R., Parada, A., and Fuhrman, J.A. (2013) Short-term observations of marine bacterial and viral communities: patterns, connections and resilience. *ISME J* **7:** 1274–1285.

Needham, D.M., and Fuhrman, J.A. (2016) Pronounced daily succession of phytoplankton, archaea and bacteria following a spring bloom. *Nat Microbiol* **1:** 16005.

Ofiţeru, I.D., Lunn, M., Curtis, T.P., Wells, G.F., Criddle, C.S., Francis, C.A., *et al.* (2010) Combined niche and neutral effects in a microbial wastewater treatment community. *Proc Natl Acad Sci USA* **107:** 15345–15350.

Ohtsubo, S., Demizu, K., Kohno, S., Miura, I., Ogawa, T., and Fukuda, H. (1992) Comparison of acetate utilization among strains of an aceticlastic methanogen, *Methanothrix soehngenii*. *Appl Environ Microbiol* **58:** 703–705.

Ovreas, L., Bourne, D., Sandaa, R.A., Casamayor, E.O., Benlloch, S., Goddard, V., *et al.* (2003) Response of bacterial and viral communities to nutrient manipulations in seawater mesocosms. *Aquat Microb Ecol* **31:** 109–121.

Paez-Espino, D., Eloe-Fadrosh, E.A., Pavlopoulos, G.A., Thomas, A.D., Huntemann, M., Mikhailova, N., *et al.* (2016) Uncovering earth's virome. *Nature* **536:** 425–430.

Peterson, G., Allen, R.C., and Holling, S.C. (1998) Ecological resilience, biodiversity, and scale. *Ecosystems* **1:** 6–18.

Raes, J., Letunic, I., Yamada, T., Jensen, L.J., and Bork, P. (2011) Toward molecular trait-based ecology through integration of biogeochemical, geographical and metagenomic data. *Mol Syst Biol* **7:** 473.

Reyes, A., Semenkovich, N.P., Whiteson, K., Rohwer, F., and Gordon, J.I. (2012) Going viral: next-generation sequencing applied to phage populations in the human gut. *Nat Rev Microbiol* **10:** 607–617.

Roden, E.E., and Jin, Q. (2011) Thermodynamics of microbial growth coupled to metabolism of glucose, ethanol, short-chain organic acids, and hydrogen. *Appl Environ Microbiol* **77:** 1907–1909.

Rodriguez-Brito, B., Li, L., Wegley, L., Furlan, M., Angly, F., Breitbart, M., *et al.* (2010) Viral and microbial community dynamics in four aquatic environments. *ISME J* **4:** 739–751.

Rodriguez-Valera, F., Martin-Cuadrado, A.B., Rodriguez-Brito, B., Pasic, L., Thingstad, T.F., Rohwer, F., *et al.* (2009) Explaining microbial population genomics through phage predation. *Nat Rev Micro* **7:** 828–836.

Rosenberg, E., Bittan-Banin, G., Sharon, G., Shon, A., Hershko, G., Levy, I., *et al.* (2010) The phage-driven microbial loop in petroleum bioremediation. *Microb Biotechnol* **3:** 467–472.

Shapiro, O.H., and Kushmaro, A. (2011) Bacteriophage ecology in environmental biotechnology processes. *Curr Opin Biotechnol* **22:** 449–455.

Shapiro, O.H., Kushmaro, A., and Brenner, A. (2010) Bacteriophage predation regulates microbial abundance and diversity in a full-scale bioreactor treating industrial wastewater. *ISME J* **4:** 327–336.

Shaw, A., Takacs, I., Pagilla, K., Riffat, R., DeClippeleir, H., Wilson, C., *et al.* (2015) Toward universal half-saturation coefficients: Describing extant k_s as a function of diffusion. *Water Environ Res* **87:** 387–391.

Sloan, W.T., Lunn, M., Woodcock, S., Head, I.M., Nee, S., and Curtis, T.P. (2006) Quantifying the roles of immigration and chance in shaping prokaryote community structure. *Environ Microbiol* **8:** 732–740.

Smith, D.P., and McCarty, P.L. (1990) Factors governing methane fluctuations following shock loading of digesters. *Res J Water Pollut Control Fed* **62:** 58–64.

Smith, S.L., Yamanaka, Y., Pahlow, M., and Oschlies, A. (2009) Optimal uptake kinetics: physiological acclimation explains the pattern of nitrate uptake by phytoplankton in the ocean. *Mar Ecol Prog Ser* **384:** 1–12.

Sommer, U. (1984) The paradox of the plankton: Fluctuations of phosphorus availability maintain diversity of phytoplankton in flow-through cultures. *Limnol Oceanogr* **29:** 633–636.

Stewart, F.M., and Levin, B.R. (1973) Partitioning of resources and the outcome of interspecific competition: A model and some general considerations. *Am Nat* **107:** 171–198.

Strom, S.L. (2008) Microbial ecology of ocean biogeochemistry: A community perspective. *Science* **320:** 1043–1045.

Sullivan, M.B., Waterbury, J.B., and Chisholm, S.W. (2003) Cyanophages infecting the oceanic cyanobacterium *Prochlorococcus*. *Nature* **424:** 1047–1051.

Suttle, C.A. (1994) The significance of viruses to mortality in aquatic microbial communities. *Microb Ecol* **28:** 237–243.

Suttle, C.A. (2007) Marine viruses – major players in the global ecosystem. *Nat Rev Microbiol* **5:** 801–812.

Thingstad, T., and Lignell, R. (1997) Theoretical models for the control of bacterial growth rate, abundance, diversity and carbon demand. *Aquat Microb Ecol* **13:** 19–27.

Thingstad, T.F. (2000) Elements of a theory for the mechanisms controlling abundance, diversity, and biogeochemical role of lytic bacterial viruses in aquatic systems. *Limnol Oceanogr* **45:** 1320–1328.

Thomas, R., Berdjeb, L., Sime-Ngando, T., and Jacquet, S. (2011) Viral abundance, production, decay rates and life strategies (lysogeny versus lysis) in Lake Bourget (France). *Environ Microbiol* **13:** 616–630.

Tilman, D. (1982) *Resource Competition and Community Structure*. Princeton, NJ: Princeton University Press.

Tilman, D. (1996) Biodiversity: population versus ecosystem stability. *Ecology* **77:** 350–363.

Tilman, D., Lehman, C.L., and Bristow, C.E. (1998) Diversity-stability relationships: Statistical inevitability or ecological consequence? *Am Nat* **151:** 277–282.

Vage, S., Storesund, J.E., and Thingstad, T.F. (2013) Adding a cost of resistance description extends the ability of virus–host model to explain observed patterns in structure and function of pelagic microbial communities. *Environ Microbiol* **15:** 1842–1852.

Vanwonterghem, I., Jensen, P.D., Dennis, P.G., Hugenholtz, P., Rabaey, K., and Tyson, G.W. (2014) Deterministic processes guide long-term synchronised population dynamics in replicate anaerobic digesters. *ISME J* **8:** 2015–2028.

Vanwonterghem, I., Jensen, P.D., Rabaey, K., and Tyson, G.W. (2016) Genome-centric resolution of microbial diversity, metabolism and interactions in anaerobic digestion. *Environ Microbiol* **18:** 3144–3158.

Vos, M., Birkett, P.J., Birch, E., Griffiths, R.I., and Buckling, A. (2009) Local adaptation of bacteriophages to their bacterial hosts in soil. *Science* **325:** 833.

Wand, U., Samarkin, V.A., Nitzsche, H.M., and Hubberten, H.W. (2006) Biogeochemistry of methane in the permanently ice-covered Lake Untersee, central Dronning Maud Land, East Antarctica. *Limnol Oceanogr* **51:** 1180–1194.

Wang, X., Wen, X., Yan, H., Ding, K., Zhao, F., and Hu, M. (2011) Bacterial community dynamics in a functionally stable pilot-scale wastewater treatment plant. *Bioresour Technol* **102:** 2352–2357.

Weinbauer, M.G. (2004) Ecology of prokaryotic viruses. *FEMS Microbiol Rev* **28:** 127–181.

Weinberger, A.D., Sun, C.L., Pluciński, M.M., Denef, V.J., Thomas, B.C., Horvath, P., *et al*. (2012) Persisting viral sequences shape microbial CRISPR-based immunity. *PLoS Comput Biol* **8:** e1002475.

Weitz, J.S. (2015) *Quantitative Viral Ecology: Dynamics of Viruses and Their Microbial Hosts. Monographs in Population Biology*. Princeton University Press. 341 pages. ISBN: 9781400873968. Princeton, USA.

Weitz, J.S., Poisot, T., Meyer, J.R., Flores, C.O., Valverde, S., Sullivan, M.B., *et al*. (2013) Phage–bacteria infection networks. *Trends Microbiol* **21:** 82–91.

Weitz, J.S., Stock, C.A., Wilhelm, S.W., Bourouiba, L., Coleman, M.L., Buchan, A., *et al*. (2015) A multitrophic model to quantify the effects of marine viruses on microbial food webs and ecosystem processes. *ISME J* **9:** 1352–1364.

Werner, J.J., Knights, D., Garcia, M.L., Scalfone, N.B., Smith, S., Yarasheski, K., *et al*. (2011) Bacterial community structures are unique and resilient in full-scale bioenergy systems. *Proc Natl Acad Sci USA* **108:** 4158–4163.

Whitman, W.B., Coleman, D.C., and Wiebe, W.J. (1998) Prokaryotes: The unseen majority. *Proc Natl Acad Sci USA* **95:** 6578–6583.

Wittebolle, L., Marzorati, M., Clement, L., Balloi, A., Daffonchio, D., Heylen, K., *et al*. (2009) Initial community evenness favours functionality under selective stress. *Nature* **458:** 623–626.

Wittebolle, L., Vervaeren, H., Verstraete, W., and Boon, N. (2008) Quantifying community dynamics of nitrifiers in functionally stable reactors. *Appl Environ Microbiol* **74:** 286–293.

Wohl, D.L., Arora, S., and Gladstone, J.R. (2004) Functional redundancy supports biodiversity and ecosystem function in a closed and constant environment. *Ecology* **85:** 1534–1540.

Xing, J., Criddle, C., and Hickey, R. (1997) Long-term adaptive shifts in anaerobic community structure in response to a sustained cyclic substrate perturbation. *Microb Ecol* **33:** 50–58.

Supporting information

Additional Supporting Information may be found in the online version of this article at the publisher's website:

Fig. S1. Phage-host trajectories. Cell concentrations (horizontal axes) and associated phage concentrations (vertical axes) across time (one plot per phage-host pair), during a simulation at 5-fold functional redundancy (i.e. comprising 60 cell populations). Rows correspond to different functional groups (names as in Fig. 1), columns correspond to different OTUs competing within a functional group. A brighter point on a trajectory indicates an earlier time in the

simulation. Trajectories that appear mostly bright correspond to hosts that went extinct early in the simulation.

Fig. S2. Effects of functional redundancy on community performance, at lowN:C ratios. (A) Temporal averages and (B) temporal coefficients of variation of effluent methane concentration, for various degrees of functional redundancy in the inoculum. In (A), also shown are cases without phages present (two right-most boxes). In all figures, box plots represent the distribution across 100 random simulations. Whiskers span 95% percentiles around the median. Simulations were performed using an N:C molar ratio in the inflow of 0.0075, which is 10 times lower than the one used in the main article.

Fig. S3. OTU composition at the community level and effluent methane. (A) Proportions of cell concentrations over time (one color per OTU) during a simulation at 20-fold functional redundancy in the inoculum. (B) Corresponding concentration of methane in the effluent. (C,D) Analogous to (A,B), but for a 100-fold functional redundancy. The first and second row correspond to Figs. 4A and 4E respectively.

Fig. S4. Effects of functional redundancy on functional community composition, at low N:C ratios. Row 1: Coefficients of variation (CV) for the proportions of (A) cell densities grouped by catabolic stage, (B) fermenting functional groups, (C) syntrophic functional groups and (D) methanogenic functional groups, at various levels of functional redundancy. Row 2: Degree of dynamic stabilization (DDS) of functional group proportions, corresponding to A–D. Box plots represent the distribution of CVs (A–D) and DDSs (E–H) across 100 random simulations; vertical bars indicate 95% percentiles. DDS was not calculated for 1x functional redundancy in E–H, as each functional group consists of only one OTU. Simulations were performed using an N:C molar ratio in the inflow of 0.0075, which is 10 times lower than the one used in the main article.

Table S1. Reaction stoichiometry. Reaction stoichiometry, standard Gibbs free energies (ΔG^{o}, $kJ \cdot mol^{-1}$ e donnor, from Conrad, 1999) and electrons transferred (γ, mol e per mol e-donor, from Roden and Jin, 2011, Table S2). Reaction IDs are as in Fig. 1.

Table S2. Model parameters. Parameters used in the model, including substrate half-saturation concentrations and maximum cell-specific substrate uptake rates. Parameters marked with an asterisk (*) are randomly and uniformly chosen within an interval spanning 10–1000 % of their default value, independently for each OTU or phage species and for each simulation. The actual parameters V, K and β for each OTU (Eqs. (4) and (9) in the main article) are set to $V = V^{o}k\lambda$, $K^{o}k/(1-k)$ and $\beta = \beta^{o}\lambda$, where k and λ are random tradeoff-parameters in (0, 1), as described in the main article.

Taxonomic variability and functional stability in microbial communities infected by phages
- Supplementary Material -

S.1 Testing the plausibility of population drift as a cause of OTU turnover

Population drift due to random birth-death events has been suggested previously as a cause of OTU turnover within functional groups over time, under constant environmental conditions (Ofiţeru *et al.*, 2010). However, the importance of drift (e.g., compared to niche-based processes and competitive exclusion) generally decreases at higher population sizes (Lande *et al.*, 2003). Even under neutral drift (i.e., in the absence of competitive differences), stochastic population trajectories may change very slowly when population sizes are high. Here, to assess the extent to which population drift could possibly explain temporal changes of natural microbial community composition, we examined a simple stochastic birth-death model for the population sizes of two competing equivalent OTUs. Using this model, we calculated the expected time it would take for an initially rare OTU to eventually become dominant solely by drift, and we compared that time with typical time scales of microbial community changes. We note that the results described below also hold if in the model we had considered more than 2 OTU populations.

The model is a discrete-time Markov chain that considers the population sizes (N_1 and N_2) of two equivalent OTUs over time. Both OTUs have equal death rates and equal birth rates, and the total population size ($N = N_1 + N_2$) is assumed to be constant. At each time step, a cell is removed ("death") from one of the two populations at random, while one of the remaining cells in any of the two populations divides, resulting in the addition of a new cell ("birth"). The probability that the removed cell belongs to population 1 is given by N_1/N. The probability that the added cell belongs to population 1 is given by $(N_1 - 1)/(N - 1)$ or $N_1/(N - 1)$, depending on whether the preceding death occurred in population 1 or 2. Hence, after each time step N_1 is either decreased by 1, increased by 1 or kept unchanged. The transition probabilities for N_1 are as follows:

$$P(i \to i+1) = \frac{i(N-i)}{N(N-1)}, \tag{1}$$

$$P(i \to i-1) = \frac{i(N-i)}{N(N-1)}, \tag{2}$$

$$P(i \to i) = 1 - \frac{2i(N-i)}{N(N-1)}, \tag{3}$$

while all other $P(i \to j)$ are zero. We mention that this model is very similar to the Moran process (without mutation or selection), which is widely used in the context of population genetics (Moran, 1958). We were specifically interested in calculating the average time that it would take for N_1 to reach a given threshold M for the first time when starting at some lower population size m ($1 \leq m < M \leq N$), conditional upon eventually reaching M. This "expected transition time" (in terms of time steps) can be calculated using standard mathematical techniques for finite Markov chains (Otto and Day, 2007, Sections 14.3.3 and 14.3.4,

recipes 14.2 and 14.4). The formulas by Otto and Day (2007) can be applied directly if M is treated as an additional "absorbing state", i.e. where $P(M \rightarrow j)$ is set to 1 for $j = M$ and 0 otherwise.

For the example cited in the main text, we conservatively considered a small total population size of $N = 10^4$, and calculated the expected transition time from $m = 0.1 \times N$ to $M = 0.9 \times N$. To translate time steps into actual time, we conservatively assumed a generation time of ~ 1 day (one time step thus corresponds to $\sim 1/N$ days), noting that in natural environments (as well as in our bioreactor model) prokaryotic generation times are typically longer (Whitman *et al.*, 1998). We found that, even with these conservative parameters, the expected transition time from low to high abundance via drift would be 6923 days. In conclusion, while in principle drift can lead to complete OTU turnover over time, in realistic microbial communities the time required for OTU turnover via drift would be much higher than typically observed turnover times, even under constant environmental conditions (days to months; Dumont *et al.*, 2009; Ofiţeru *et al.*, 2010; Rodriguez-Brito *et al.*, 2010).

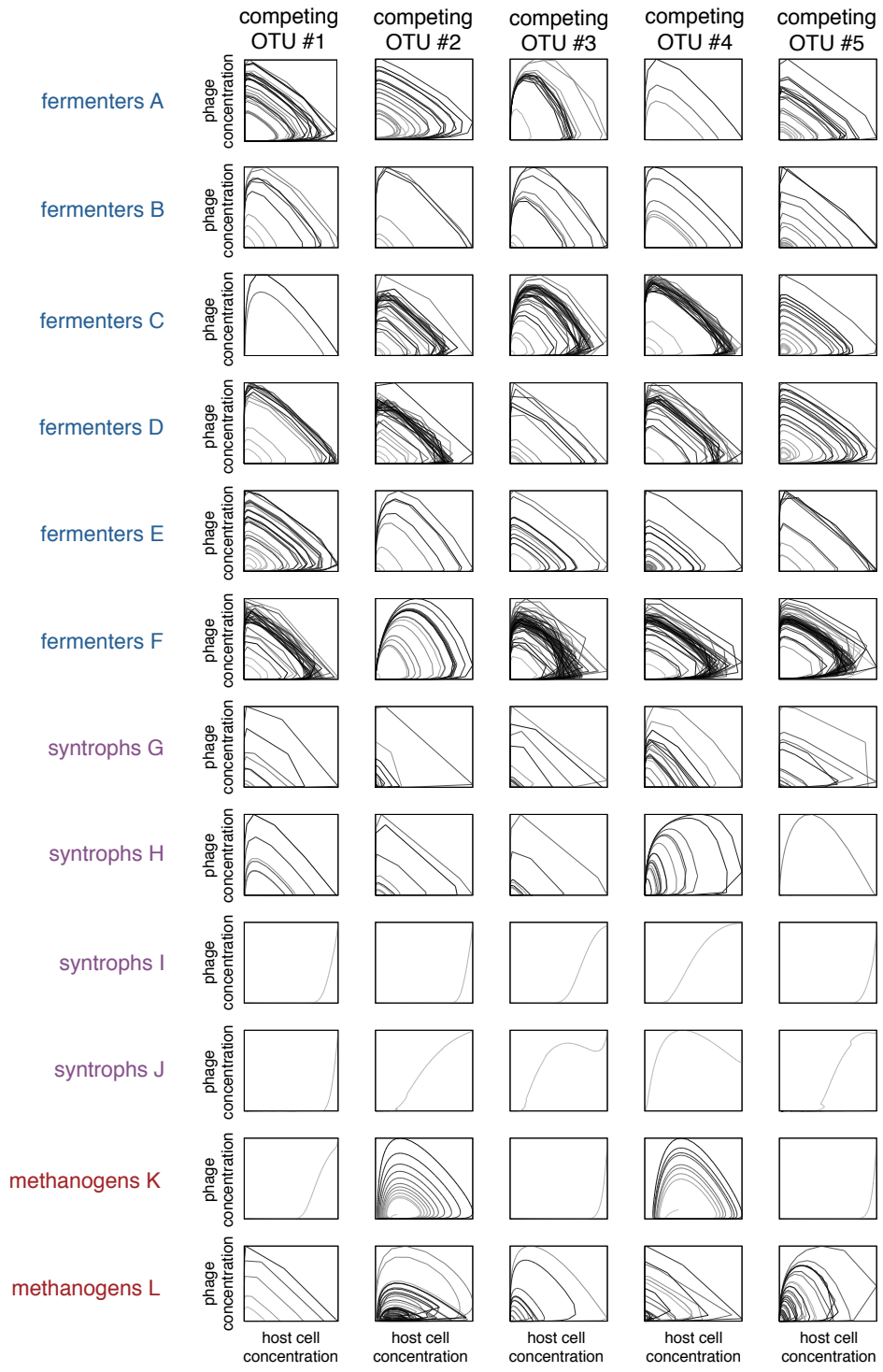

Figure S1: **Phage-host trajectories.** Cell concentrations (horizontal axes) and associated phage concentrations (vertical axes) across time (one plot per phage-host pair), during a simulation at 5-fold functional redundancy (i.e., comprising 60 cell populations). Rows correspond to different functional groups (names as in Fig. 1), columns correspond to different OTUs competing within a functional group. A brighter point on a trajectory indicates an earlier time in the simulation. Trajectories that appear mostly bright correspond to hosts that went extinct early in the simulation.

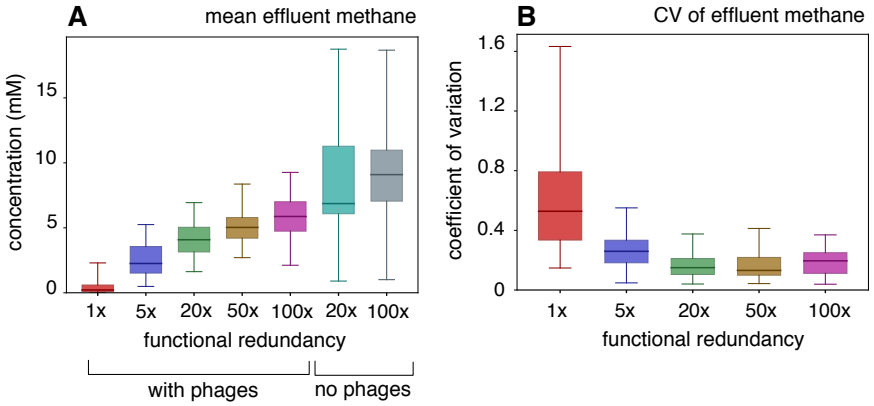

Figure S2: **Effects of functional redundancy on community performance, at low N:C ratios.** (A) Temporal averages and (B) temporal coefficients of variation of effluent methane concentration, for various degrees of functional redundancy in the inoculum. In (A), also shown is the case without phages present (right-most box). In all figures, box plots represent the distribution across 100 random simulations. Whiskers span 95% percentiles around the median. Simulations were performed using an N:C molar ratio in the inflow of 0.0075, which is 10 times lower than the one used in the main article.

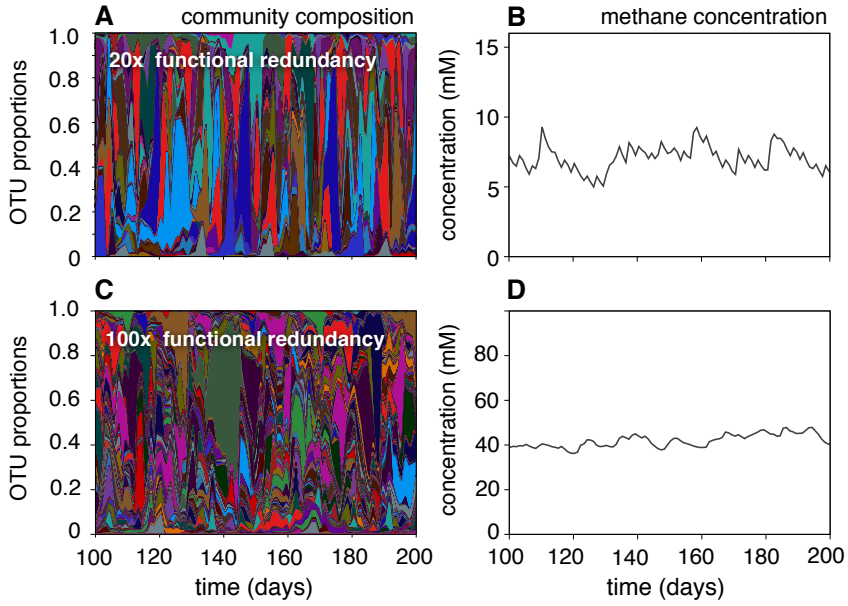

Figure S3: **OTU composition at the community level and effluent methane.** (A) Proportions of cell concentrations over time (one color per OTU) during a simulation at 20-fold functional redundancy in the inoculum. (B) Corresponding concentration of methane in the effluent. (C,D) Analogous to (A,B), but for a 100-fold functional redundancy. The first and second row correspond to Figs. 4A and 4E, respectively.

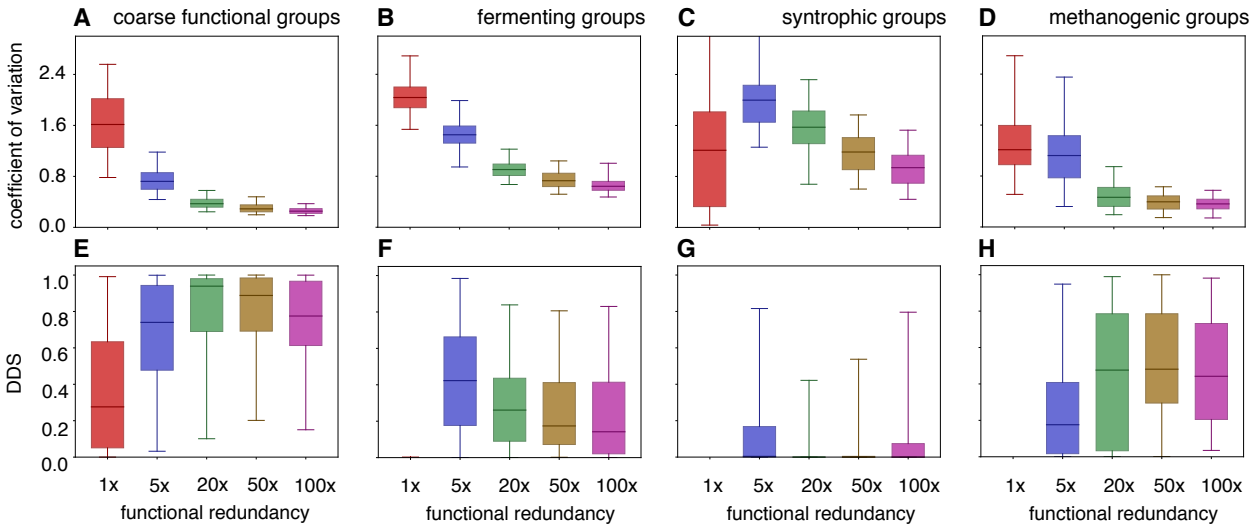

Figure S4: **Effects of functional redundancy on functional community composition, at low N:C ratios.** Row 1: Coefficients of variation (CV) for the proportions of (A) cell densities grouped by catabolic stage, (B) fermenting functional groups, (C) syntrophic functional groups and (D) methanogenic functional groups, at various levels of functional redundancy. Row 2: Degree of dynamic stabilization (DDS) of functional group proportions, corresponding to A–D. Box plots represent the distribution of CVs (A–D) and DDSs (E–H) across 100 random simulations; vertical bars indicate 95% percentiles. DDS was not calculated for 1x functional redundancy in E–H, as each functional group consists of only one OTU. Simulations were performed using an N:C molar ratio in the inflow of 0.0075, which is 10 times lower than the one used in the main article.

Table S1: **Reaction stoichiometry.** Reaction stoichiometry, standard Gibbs free energies (ΔG^o, $\mathrm{kJ \cdot mol^{-1}}$ e donnor, from Conrad, 1999) and electrons transferred (γ, mol e per mol e-donor, from Roden and Jin, 2011, Table S2). Reaction IDs are as in Fig. 1.

ID	Reaction	ΔG^o	γ
	glucose fermentation		
A	$C_6H_{12}O_6 \rightarrow 2\ CH_3CH_2OH + 2\ CO_2$	-235.0	24
B	$C_6H_{12}O_6 \rightarrow 2\ CH_3CHOHCOOH$	-198.1	24
C	$C_6H_{12}O_6 \rightarrow 3\ CH_3COOH$	-311.2	24
D	$C_6H_{12}O_6 + 2\ H_2O \rightarrow 2\ CH_3COOH + 2\ CO_2 + 4\ H_2$	-216.1	24
E	$C_6H_{12}O_6 \rightarrow 4/3\ CH_3CH_2COOH + 2/3\ CH_3COOH + 2/3\ CO_2 + 2/3\ H_2O$	-311.4	24
F	$C_6H_{12}O_6 \rightarrow 2/3\ CH_3CH_2CH_2COOH + 2/3\ CH3COOH + 2\ CO_2 + 8/3\ H_2$	-248.0	24
	syntrophy (catabolism of short-chain fatty acids, lactate and alcohols)		
G	$CH_3CH_2OH \rightarrow CH_3COOH + 2\ H_2$	$+9.6$	12
H	$CH_3CHOHCOOH + H_2O \rightarrow CH_3COOH + CO_2 + 2\ H_2$	-48.7	12
I	$CH_3CH_2COOH + 2\ H_2O \rightarrow CH_3COOH + CO_2 + 3\ H_2$	$+31.8$	14
J	$CH_3CH_2CH_2COOH + 2\ H_2O \rightarrow 2\ CH_3COOH + 2\ H_2$	$+48.3$	20
	methanogenesis		
K	$CH_3COOH \rightarrow CO_2 + CH_4$	-35.6	8
L	$H_2 + (1/4)\ CO_2 \rightarrow (1/2)\ H_2O + (1/4)\ CH_4$	-32.7	2

Table S2: **Model parameters.** Parameters used in the model, including substrate half-saturation concentrations and maximum cell-specific substrate uptake rates. Parameters marked with an asterisk ($\star$) are randomly and uniformly chosen within an interval spanning 10–1000 % of their default value, independently for each OTU or phage species and for each simulation. The actual parameters V, K and β for each OTU (Eqs. (4) and (9) in the main article) are set to $V = V^o\kappa\lambda$, $K^o\kappa/(1-\kappa)$ and $\beta = \beta^o\lambda$, where κ and λ are random tradeoff-parameters in $(0, 1)$, as described in the main article.

symbol and description		scope		default value	ref.
m	dry cell mass	fermenters		280 fg	a
	— " —	syntrophs		280 fg	a
	— " —	H_2/CO_2 methanogens		440 fg	b
	— " —	acetoclastic methanogens		2.5 pg	b
V^o	max. cell-sp. glucose upt. rate	fermenters	$\star$	67.2 fmol/(cell · d)	c†
K^o	glucose half-saturation conc.	— " —	$\star$	0.53 mM	c†
V^o	max. cell-sp. H_2 upt. rate	H_2/CO_2 methanogens	$\star$	1.43 pmol/(cell · d)	b
K^o	H_2 half-saturation conc.	— " —	$\star$	7.65 μM	b
V^o	max. cell-sp. acetate upt. rate	acetoclastic methanogens	$\star$	0.55 pmol/(cell · d)	b
K^o	acetate half-saturation conc.	— " —	$\star$	442 μM	b
V^o	max. cell-sp. lactate upt. rate	lactate syntrophs	$\star$	143 fmol/(cell · d)	d†
K^o	lactate half-saturation conc.	— " —	$\star$	380 μM	d
V^o	max. cell-sp. ethanol upt. rate	ethanol syntrophs	$\star$	536 fmol/(cell · d)	e†
K^o	ethanol half-saturation conc.	— " —	$\star$	0.3 μM	f
V^o	max. cell-sp. butyrate upt. rate	butyrate syntrophs	$\star$	72.8 fmol/(cell · d)	d†
K^o	butyrate half-saturation conc.	— " —	$\star$	76 μM	b
V^o	max. cell-sp. propionate upt. rate	propionate syntrophs	$\star$	44.8 fmol/(cell · d)	d†
K^o	butyrate half-saturation conc.	— " —	$\star$	432 μM	g
β^o	phage infectivity	free phage particles	$\star$	3×10^{-10} L/d	h,i
δ	phage inactivation rate	— " —	$\star$	0.48 d^{-1}	j
μ	lysis rate	all infected cells	$\star$	6 d^{-1}	i,k
ν	lysis burst size	— " —	$\star$	24	i,k
λ	hydraulic turnover rate	bioreactor		0.1 d^{-1}	l
C^o_{gl}	glucose input concentration	bioreactor		1 g/L	l,m
T	temperature	bioreactor		35°C	k
pH		bioreactor		7.0	l
$\Delta\Psi$	membrane electric potential	all cells		120 mV	n
Y	biomass yield	fermentation to H_2+acet.+butyrate		15.6 g dW/mol gluc.	o
	— " —	fermentation to ethanol		7.04 g dW/mol gluc.	p
	— " —	fermentation to acet.+propionate		8.65 g dW/mol gluc.	p
	— " —	fermentation to lactate		6.26 g dW/mol gluc.	p
	— " —	fermentation to acetate		8.64 g dW/mol gluc.	p
	— " —	fermentation to H_2+acet.		6.64 g dW/mol gluc.	p
	— " —	lactate syntrophy		4.60 g dW/mol lact.	o
	— " —	ethanol syntrophy		3.45 g dW/mol eth.	o
	— " —	butyrate syntrophy		0.996 g dW/mol but.	o
	— " —	propionate syntrophy		1.31 g dW/mol prop.	o
	— " —	H_2/CO_2 methanogenesis		1.08 g dW/mol H_2	o
	— " —	acetoclastic methanogenesis		1.73 g dW/mol ac.	o
D_{amm}	ammonium diffusion coeff.	bioreactor		23.955×10^{-10} m^2/s	q
R_{c}	cell radius	all cells		0.546 μm	r

a: Neidhardt and Umbarger, 1996. b: Ahring and Westermann, 1987. c: Meadows *et al.*, 2010. d: Costello *et al.*, 1991. e: Courtin and Spoelstra, 1990. f: Kalyuzhnyi, 1997. g: Lawrence and McCarty, 1969. h: Abedon, 1989. i: Middelboe *et al.*, 2001. j: Suttle, 1994; Ottosson and Stenström, 2003; Fischer *et al.*, 2004. k: Meile *et al.*, 1989. l: Xing *et al.*, 1997; Fernández *et al.*, 1999. m: Jones *et al.*, 1995; Wand *et al.*, 2006. n: LaRowe *et al.*, 2012; Reed *et al.*, 2014. o: Table S2 in Roden and Jin (2011). p: Inserting ΔG^o from Table S1 into the regression formula by Roden and Jin (2011). q: Table 4.7 in Boudreau, 1997. r: based on exponentially growing *E. coli* (Kubitschek and Bendigkeit, 1955). †: Mass-specific rates converted to cell-specific rates based on a dry cell mass of 2.8×10^{-13} g (Neidhardt and Umbarger, 1996).

References

Abedon, S.T. (1989) Selection for bacteriophage latent period length by bacterial density: A theoretical examination. *Microb Ecol* **18**: 79–88.

Ahring, B.K. and Westermann, P. (1987) Kinetics of butyrate, acetate, and hydrogen metabolism in a thermophilic, anaerobic, butyrate-degrading triculture. *Appl Environ Microbiol* **53**: 434–439.

Boudreau, B.P. (1997) Diagenetic models and their implementation; modelling transport and reactions in aquatic sediments. Springer.

Conrad, R. (1999) Contribution of hydrogen to methane production and control of hydrogen concentrations in methanogenic soils and sediments. *FEMS Microbiol Ecol* **28**: 193–202.

Costello, D., Greenfield, P., and Lee, P. (1991) Dynamic modelling of a single-stage high-rate anaerobic reactor—II. Model verification. *Water Res* **25**: 859–871.

Courtin, M.G. and Spoelstra, S.F. (1990) A simulation model of the microbiological and chemical changes accompanying the initial stage of aerobic deterioration of silage. *Grass Forage Sci* **45**: 153–165.

Dumont, M., Harmand, J., Rapaport, A., and Godon, J.J. (2009) Towards functional molecular fingerprints. *Environ Microbiol* **11**: 1717–1727.

Fernández, A., Huang, S., Seston, S., Xing, J., Hickey, R., Criddle, C., *et al.* (1999) How stable is stable? Function versus community composition. *Appl Environ Microbiol* **65**: 3697–3704.

Fischer, U.R., Weisz, W., Wieltschnig, C., Kirschner, A.K.T., and Velimirov, B. (2004) Benthic and pelagic viral decay experiments: a model-based analysis and its applicability. *Appl Environ Microbiol* **70**: 6706–6713.

Jones, J.B., Holmes, R.M., Fisher, S.G., Grimm, N.B., and Greene, D.M. (1995) Methanogenesis in Arizona, USA dryland streams. *Biogeochemistry* **31**: 155–173.

Kalyuzhnyi, S. (1997) Batch anaerobic digestion of glucose and its mathematical modeling. II. Description, verification and application of model. *Bioresour Technol* **59**: 249–258.

Kubitschek, H. and Bendigkeit, H. (1955) Some studies on the growth and size of bacteria. *Quarterly Report of Biological and Medical Research Division, Argonne National Laboratory. ANL-5426* pp. 99–109.

Lande, R., Engen, S., and Sæther, B. (2003) Stochastic Population Dynamics in Ecology and Conservation. Oxford series in ecology and evolution. Oxford University Press.

LaRowe, D.E., Dale, A.W., Amend, J.P., and Van Cappellen, P. (2012) Thermodynamic limitations on microbially catalyzed reaction rates. *Geochim Cosmochim Acta* **90**: 96–109.

Lawrence, A.W. and McCarty, P.L. (1969) Kinetics of methane fermentation in anaerobic treatment. *Water Pollution Control Federation* **41**: R1–R17.

Meadows, A.L., Karnik, R., Lam, H., Forestell, S., and Snedecor, B. (2010) Application of dynamic flux balance analysis to an industrial *Escherichia coli* fermentation. *Metab Eng* **12**: 150–160.

Meile, L., Jenal, U., Studer, D., Jordan, M., and Leisinger, T. (1989) Characterization of ψm1, a virulent phage of *Methanobacterium thermoautotrophicum* Marburg. *Arch Microbiol* **152**: 105–110.

Middelboe, M., Hagström, A., Blackburn, N., Sinn, B., Fischer, U., Borch, N., *et al.* (2001) Effects of bacteriophages on the population dynamics of four strains of pelagic marine bacteria. *Microb Ecol* **42**: 395–406.

Moran, P.A.P. (1958) Random processes in genetics. *Math Proc Cambridge Philos Soc* **54**: 60–71.

Neidhardt, F.C. and Umbarger, H.E. (1996) Chemical composition of *Escherichia coli*. In N. F.C. (ed.) Escherichia coli and Salmonella: Cellular and Molecular Biology, volume 1, 2nd edition, chapter 3. American Society of Microbiology (ASM) Press.

Ofiţeru, I.D., Lunn, M., Curtis, T.P., Wells, G.F., Criddle, C.S., Francis, C.A., *et al.* (2010) Combined niche and neutral effects in a microbial wastewater treatment community. *Proc Natl Acad Sci USA* **107**: 15345–15350.

Otto, S.P. and Day, T. (2007) A biologist's guide to mathematical modeling in ecology and evolution, volume 13. Princeton University Press.

Ottosson, J. and Stenström, T.A. (2003) Growth and reduction of microorganisms in sediments collected from a greywater treatment system. *Lett Appl Microbiol* **36**: 168–172.

Reed, D.C., Algar, C.K., Huber, J.A., and Dick, G.J. (2014) Gene-centric approach to integrating environmental genomics and biogeochemical models. *Proc Natl Acad Sci USA* **111**: 1879–1884.

Roden, E.E. and Jin, Q. (2011) Thermodynamics of microbial growth coupled to metabolism of glucose, ethanol, short-chain organic acids, and hydrogen. *Appl Environ Microbiol* **77**: 1907–1909.

Rodriguez-Brito, B., Li, L., Wegley, L., Furlan, M., Angly, F., Breitbart, M., *et al.* (2010) Viral and microbial community dynamics in four aquatic environments. *ISME J* **4**: 739–751.

Suttle, C.A. (1994) The significance of viruses to mortality in aquatic microbial communities. *Microb Ecol* **28**: 237–243.

Wand, U., Samarkin, V.A., Nitzsche, H.M., and Hubberten, H.W. (2006) Biogeochemistry of methane in the permanently ice-covered Lake Untersee, central Dronning Maud Land, East Antarctica. *Limnol Oceanogr* **51**: 1180–1194.

Whitman, W.B., Coleman, D.C., and Wiebe, W.J. (1998) Prokaryotes: The unseen majority. *Proc Natl Acad Sci USA* **95**: 6578–6583.

Xing, J., Criddle, C., and Hickey, R. (1997) Long-term adaptive shifts in anaerobic community structure in response to a sustained cyclic substrate perturbation. *Microb Ecol* **33**: 50–58.